INSTITUTE FOR GEOSCIENCE

Center for Applied Geoscience (ZAG)

Master Thesis

Master of Science (M.Sc.) in
Applied Environmental Geoscience (AEG)

Avneesh Nayal

Development of a visibility criterion for marine discharge of Iron-rich mine water

Supervisors

Prof. Dr. Christian Wolkersdorfer
Dr. Philipp Blum

Tübingen, October 2009

I hereby certify that the work written and presented within this thesis was conducted solely by me, with the aid of the references listed.

October, 2009 Avneesh Nayal

Acknowledgments

Sincere gratitude to my supervisor Professor Dr. Christian Wolkersdorfer for giving me the opportunity to travel to Canada and conduct research at the Mine Water Remediation and Management group at Cape Breton University. Working under him was truly inspiring and a great learning experience.

I am grateful to Dr. Ross F. McCurdy, President of the Cape Breton Development Corporation, for providing the funding and hence the opportunity to conduct this interesting research.

Furthermore, I would like to thank my colleagues in Canada: Beth Maclellan, Elyse Gregor, Mackenzie Turner, Martina Ueckert, Maximilian Reitzel and Michelle Prendergast for providing scientific support and enormous friendly assistance whenever needed.

I also thank Dr. Philipp Blum (University of Tübingen) for his invaluable guidance and supervision during the writing of this work.

Contents

Abstract **4**

1 Introduction **5**

1.1 Water in mining 5

1.2 Hydrogeochemistry of mine water 5

1.3 Previous work 7

1.4 Objectives of this study 10

2 Materials and Methods **11**

2.1 Synthetic mine water 11

2.1.1 Composition 11

2.1.2 Recalibration 12

2.2 Batch experiments 12

2.3 Tank experiments 14

2.3.1 Synthesizing mine water flow 16

2.3.2 Synthesizing oceanic mixing 18

2.4 Turbidity measurements 18

2.5 Iron measurements 18

3 Results and Discussion **20**

3.1 Batch experiments 20

3.2 Tank experiments 28

3.2.1 Concentration based limit 28

3.2.2 Stability 30

3.2.3 Visual assessment 31

3.2.4 Emulating mine water discharge 31

3.3 Hydrogeochemical modeling 34

4 Conclusion **43**

References **46**

Appendix **49**

ABSTRACT

Iron coloration of surface waters due to acid mine drainage is a major cause of environmental concern, mainly due to its unsightly appearance and aesthetic aversion. This thesis investigates the visibility of such iron rich plumes in context of marine disposal of mine water using laboratory experiments with synthetic mine water mixed with seawater. The primary objective of the study is to determine a concentration and a daily load discharge limit below which no iron plume would be visible on the ocean surface, upon discharge. Furthermore, hydrogeochemistry of this mixed system is studied using the hydrogeochemical modeling program PHREEQC. Ferrous sulfate solutions were mixed with seawater samples at different ratios on small batch and large tank scales. Turbidity, electrical conductivity, total iron and pH were monitored at regular intervals along with digital photography. Based on the turbidity levels, a visual impact scale was defined. It was found that 100 mgL^{-1} ferrous iron solutions show very low fluctuation in turbidity. In contrast, higher concentrations reveal dark coloration of the mixture with high turbidity levels (> 250 Formazine Attenuation Units (FAU)). Using the site-specific discharge rate of mine water at Cadegan Brooke of 200 Ls^{-1} and by suggesting a precautionary concentration of 50 mgL^{-1}, a daily maximum iron(total) load of 864 kg/day is suggested. Results from the hydrogeochemical modeling suggest that the mixing phenomenon occurs under steady-state chemical kinetics, indicating conventional mixing. Future improvements in experiments such as high quality visual recording and large scale field experiments are also suggested.

1 INTRODUCTION

1.1 Water in mining

Mining is an essential economic activity for developed and developing countries alike. However, mine water has been and still is a cause of major environmental concern, where contaminated mine water enters the hydro-, bio- and/or anthroposphere. While in small mining regions, mine water discharges have been considered to be of no major threat, in most of the developed and developing world, the need for mine water treatment is crucial (Wolkersdorfer, 2002).

Environmental pollution of mine water can be described as falling under the categories of salinization, metal toxicity, acidity and sedimentation (Gray, 1996). Although the environmental threat of mine water diminishes within a few decades of the 'first flush', the initial years pose a high threat, especially with regard to intense release of dissolved iron concentrations (Wood et al., 1999).

1.2 Hydrogeochemistry of mine water

According to Tiwary (2001), one of the major causes of water pollution is the high acidity caused by the oxidation of sulfur bearing minerals such as pyrite (FeS_2). In coal mines, the exposure of pyrite to oxygen, due to atmospheric oxygen or dissolved oxygen results in chain of reactions causing low pH and SO_4^{2-} rich water. The chain of equations that initiate this reaction is as follows (Wolkersdorfer, 2008):

$$2FeS_2(s) + 7O_2(g) + 2H_2O(l) \rightarrow 2Fe^{2+}(aq) + 4{SO_4}^{2-}(aq) + 4H^+(aq) \quad (1)$$

$$4Fe^{2+}(aq) + O_2(g) + 4H^+(aq) \rightarrow 4Fe^{3+}(aq) + 2H_2O(l) \quad (2)$$

$$FeS_2(s) + 14Fe^{3+}(aq) + 8H_2O(l) \rightarrow 15Fe^{2+}(aq) + 2{SO_4}^{2-}(aq) + 16H^+(aq) \quad (3)$$

Equations 1-3 describe the overall oxidation process for pyrite (FeS_2), which results in the release of ferrous (Fe^{2+}) iron in the aquatic environment. Equation 1 portrays the initial exposure of the pyrite mineral to the atmosphere (or dissolved oxygen in water), which releases reduced Fe^{2+} in solution. This is accompanied by 2 protons (H^+) per mole of pyrite, which results in a significant decrease in pH. The next step in the reaction is the oxidation of Fe^{2+} to Fe^{3+} iron. This

mechanism is illustrated by Equation 2, where Fe^{2+} reacts with O_2 in the presence of 4 H^+ protons to produce Fe^{3+}.

Equation 3 describes the step that causes the largest problem with regard to an acidic mine water environment. In this step the Fe^{3+} reacts further with more pyrite to oxidize it, leading to the release of sulfate ions, Fe^{2+} and 16 protons. These 16 protons further reduce the pH of the solution dramatically and create extremely acidic waters. The additional Fe^{2+} produced, reacts further with oxygen according to Equation 2 leading to a chain reaction, which takes place at a high rate in an oxic environment.

According to Watten et al. (2005), the released ferric iron is then hydrolized to form insuluble ferric hydroxide ($Fe(OH)_3$). These ferric hydroxides and oxyhydroxides are often termed as *ochre* and can stain surface waters, sediments and land surfaces due to their bright reddish brown/orange color (Younger et al., 2002). The major iron group minerals composing ochre consist of goethite (yellowish brown), lepidocrocite (orange), ferrihydrite (reddish brown), schwertmannite (yellow) and jarosite (straw yellow); (Wolkersdorfer, 2008). Figure 1 shows an aerial image of an iron rich ochre plume migrating out into the ocean from a mine water discharge location at the 1B shaft, Glace Bay, Cape Breton Island, Nova Scotia, Canada.

Figure 1: *Aerial image showing an ochre slick/plume migrating outwards into the ocean from a mine water discharge location. Location: 1B shaft, Glace Bay, Cape Breton Island, Nova Scotia, Canada (Shea, 2008).*

1.3 Previous work

According to Jarvis and Younger (2000), environmental assessment was performed to quantify the chemical, ecological and visual impact of mine water discharges. These assessments involved the setting up of a multi phase method. The first phase addressed the impact of mine water discharges on receiving water bodies by means of physiochemical parameter assessment. Applied for the first time in South Wales, this method involved measuring of parameters such as area affected, the length affected, iron deposition (visual intensity), pH and total iron concentration.

The parameter of interest, with respect to this work, is the visual intensity of iron deposition. This was categorized into 3 classes as *high*, *medium* and *low* (Davies et al., 1997). An example of this assessment method is given in Table 1. However, the assessment was made using a ranking system, by listing the parameters in order of decreasing importance (top to bottom). As seen from Table 1, the visual impact of iron deposition falls fourth in the list, proving that it was not given much importance to, in this assessment method. In addition, Davies et al. (1997) stated that only a "subjective measurement of color intensity and degree of flocculants deposit was recorded". This further demonstrates the view that more research into the actual *visual* and *aesthetic* impact of mine water discharge should be conducted.

Table 1: *Environmental impact assessment method showing grading of physiochemical data for impact of ferruginous mine water (Davies et al., 1997).*

Impact criteria	High (A)	Medium (B)	Low (C)	No impact (D)
In order of decreasing importance				
1. Area affected (m^2)	>2500	10-2500	<10	-
2. Length affected (km)	>0.5	0.01-0.05	<0.1	-
3. Substrate quality for salmonid reproduction	Rocks/ stones/ gravel	Bedrock/ boulders/ rocks	Artificial channel sand/silt	-
4. Iron deposition (visual)	High	Medium	Low	-
5. Total iron (mg/L)	>3.0	2-3	<2.0	-
6. pH, DO (%), total Al (mg/L)	3 failures	2 failures	1 failure	No failures

Banks and Banks (2001) discussed another scoring based algorithm called the Multi Attribute Technique (MAT), which is based on a similar physico-chemical ranking system, as mentioned before, but heavier weighting is given to socio-economic factors and *aesthetic impacts* such as *recreation* and *visibility*.

The most comprehensive study conducted until now, on establishing a criterion for the discharge of mine water into the environment was performed by Younger (2008). In his study he discusses the importance of establishing a criterion, specifically for discharge of mine water into a *marine environment*. A distinguishable criterion for marine water is important, because freshwater environments differ greatly from any saltwater environment with respect to many physico-chemical parameters, especially the ionic strength, density and chlorine content. He provides a comprehensive overview of various case studies, which encountered the problem of iron 'ochre' plumes forming in marine waters (e.g. Figure 1). In the category of non-coal mines, the case of the Wheal Jane Sn/Zn mine in Cornwall, UK, monitoring and modeling resulted in the finding that a plume was visible at loading levels above ≈ 3000 kg/day of total Fe. Unfortunately, the details on how such a criterion was determined were not provided. In order to remediate this iron generated plume and due to the need of stringent regulations, the Environmental Agency in the UK set a limit of only 151 kg/day (pumping rate: 350 Ls^{-1} at concentration: 10 mgL^{-1}). In another instance, from Skinningrove, Cleveland, UK, it is suggested that no plume was visible at a concentration of 17 mgL^{-1} at a loading rate of 67 kg/day.

With reference to coal mines, in the case of the East Fife Coalfield, Scotland, mine water was being pumped directly into the ocean after the mine closure phase. Out of the 2 main shafts (Michael and Frances Shaft), discharge from the Michael Shaft at 34 mgL^{-1} Fe and a loading of 816 kg Fe/day resulted in a plume, whereas discharge from the Frances Shaft at a concentration of 12 mgL^{-1} and a loading of 108 kg Fe/day caused no visible plume. However, during *active* mining at the same location, a total loading of 924 kg Fe/day from both the shafts did not result in an ochreous plume.

Based on these and other observations of mine water discharge limits, Younger (2008) suggested a maximum daily load of 200 kg/day or 2314.8 mg/s total Fe. Using this limit as the target load and by using the anticipated flow rate (Q_{Max}, L/s), a discharge concentration of iron (Fe_{Max}, mg/L) could be calculated by using the following formula:

$$Fe_{Max} = 2314.8/Q_{Max} \quad \textbf{(4)}$$

Studies investigating the oxidation and precipitation of ferrous iron were previously performed. However, an experimental setup to investigate the mixing of mine water and ocean water has not been performed yet. A similar experiment as in the current study was setup by Kirby and Brady (1998), who used a continuously-stirred tank reactor (CSTR). The objectives of their study were to introduce the design of a field continuously-stirred tank reactor and to determine ferrous iron oxidation rates in various treated and untreated mine water samples. The CSTR design involved features different from the current study such as the inclusion of an inlet-outlet system to maintain steady state flow through the system. In addition, O_2 levels were modified by pumping compressed oxygen. Furthermore, the pH of the system was modified by addition of NaOH solutions.

Sholkovitz (1976) investigated the products (flocculants) formed as a result of filtered river water mixing with filtered seawater. The research involved investigation of the composition of flocculants of Fe, Mn, Al, P, organic carbon and humic substances. The procedure involved mixing of filtered river water with filtered seawater at different salinities and then letting the mixture stand undisturbed for a set time period. Thereafter, the flocculants were filtered and analyzed for Fe, Mn, Al, P, Si, Ti and humates using thin film X-ray fluorescence. A similar study that investigated the removal of iron from a mixture of river water and seawater was published by Boyle et al. (1977). Other studies include the investigation of concentration change of soluble and particulate iron in seawater (Lewin and Chen, 1973), investigation of iron solubility in seawater with temperature, pH and salinity dependence (Liu and Millero, 2002) and the kinetics of ferrous iron in sweater over changing pH (Roekens and Van Grieken, 1983).

Although an ecological impact assessment is not part of this current study, it should be mentioned that the ecological and toxicological impacts of such iron plumes in the ocean have been investigated and debated upon. Somerfield et al. (1994) investigated the impact of an instantaneous flooding of mine water into a neighboring creek on the benthic community populations, specifically the meio- and macro-fauna communities. In January 1992, the collapse of an adit plug in the abandoned Wheal Jane tin mine (Cornwall, UK) resulted in a flood of about 45×10^6 L of acidic mine water. This caused an ochre plume in the receiving creek. A sediment

analysis was conducted that revealed that no major change in the faunal populations was caused. The minor changes in population were attributed to seasonal fluctuations.

In the process of preventing any ecotoxicological damage, the limit on the discharge concentration of Fe is 0.1 mgL^{-1} and Zn is 0.2 mgL^{-1} in the case of Britannia Mine, British Columbia (Younger, 2008), which is not very logical when considering the higher toxicity of Zn as compared to Fe. The same problem occurred with the limit of Al discharge, which was set to an upper limit of 1.0 mgL^{-1} despite its ecotoxicological nature.

1.4 Objectives

This study deals with remediation from an aesthetic perspective. This does not imply that other threats and problems related to mine water pollution are insignificant. However, this study deals with only the visual impact of mine water discharge into the ocean. Hence, only relevant scientific techniques were applied to solve this issue. Since such an analysis is very subjective, an organoleptic study was performed to determine an estimated visibility limit and a daily iron loading limit for the discharge of mine water into the open ocean.

The objective of this study was to determine an upper limit, at which mine water upon mixing with seawater, does not generate an ochre colored slick or plume. In this context, laboratory based batch and tank experiments at increasing scales were performed. The color intensity of the various mixtures in the tanks was recorded. Solutions of different Fe(II) concentrations were also analyzed with regard to how stable (least fluctuating) their turbidity profiles were. In addition, hydrogeochemical modeling of the mixing of synthetic mine water with seawater was undertaken. Investigations were carried out to quantify the visible color changes and chemical states of the iron rich water and seawater mixture.

2 MATERIAL AND METHODS

2.1 Synthetic Mine Water

2.1.1 Composition

In order to simulate iron rich mine water in the laboratory, Fe rich solution or 'synthetic mine water' was created using $FeSO_4 \cdot 7H_2O$ (Sigma-Aldrich© iron(II) sulfate heptahydrate, CAS# 7782-63-0). For this initial small scale test, Fe(II) concentrations of 1, 10, 32, 100, 317 and 700 mgL^{-1} were chosen. Table 2 shows the range of used concentrations of Fe(II) and the corresponding mass of added $FeSO_4 \cdot 7H_2O$. The blue/green crystalline sample powder was taken in a metal spatula and then measured carefully upon a weighing balance with an accuracy of 0.0001 g. Special care was taken that the weighing was done fast with minimum exposure to the atmosphere. Thereafter, the measured powder was diluted with 1 L of distilled water.

Table 2: *Concentrations used and corresponding mass of added $FeSO_4 \cdot 7H_2O$.*

Fe(II), mgL^{-1}	$FeSO_4 \cdot 7H_2O$, mg
1	4.9
10	49.8
32	159.3
100	497.8
317	1578.1
700	3484.8

2.1.2 Re-calibration

Due to limited laboratory resources in the initial stage of this study, the ferrous sulfate chemical compound used in the experiments came from 2 different sources. During the course of the experiments, it was suspected that the used ferrous sulfate compounds were not pure. In order to calculate the actual empirical formula for the compound, a re-calibration was performed. By creating standard Fe(II) solutions with different masses of $FeSO_4$ and by measuring the total iron concentration in them, the actual formula for the compound was determined to be $FeSO_4 \cdot (2.9)H_2O$ for the first batch and $FeSO_4 \cdot (7.5)H_2O$ for the second. Table 3 shows the target concentrations and the actual measured concentrations for the 2 compounds.

Table 3: *Target (planned) ferrous iron concentrations compared to the actual (measured) concentrations in solutions of the 2 different ferrous sulfate compounds.*

Fe(II), mgL^{-1} (Planned target concentration)	Fe(II), mgL^{-1} (measured using $FeSO_4 \cdot (2.9)H_2O$)	Fe(II), mgL^{-1} (measured using $FeSO_4 \cdot (7.5)H_2O$)
1	1.7	0.97
10	13.6	9.7
32	43.6	30.9
100	136.2	96.8
317	431.7	307.1
700	953.3	678.0

2.2 Batch experiments

In order to address the issue experiments were conducted on a small scale (250 mL beakers) and on a larger scale (185 L tank). The first set of experiments involved mixing different concentrations of synthetic mine water (from laboratory created Fe(II) solutions) with 100 mL of seawater. Batch experiments were conducted for each of the above mentioned concentrations over a time period of 1 to 5 hours. The following procedure was followed for each of the 6 concentrations:

i) 5 VWR® Griffin – Low Form Beakers (250 mL borosilicate glass) were filled with 100 mL seawater.

ii) Beaker 1, placed upon a magnetic hotplate, was spiked with 1 mL of synthetic mine water using a 100–1000 µL pipette (VWR Signature™ Ergonomic High Performance Single-Channel Variable Volume Pipettors).

iii) Using a magnetic stirrer, the seawater and mine water mixture was stirred for 10 seconds or in the case of higher concentrations until the mixture appeared to be well mixed.

iv) The beaker was taken off the hotplate and 25 mL of the mixture was transferred into a HACH 25 mL sample cell.

v) The HACH DR890 colorimeter was zeroed with seawater blank, following which, turbidity of the prepared sample mixture was measured in Formazine Attenuation Units (FAU).

vi) Beaker 2 was placed on the magnetic hotplate and spiked with 3 mL of synthetic mine water.

vii) Step (iii), (iv) and (v) were repeated.

viii) Beaker 3 was placed on the magnetic hotplate and spiked with 10 mL of synthetic MW.

ix) Step (iii), (iv) and (v) were repeated.

x) Beaker 4 was placed on the magnetic hotplate and spiked with 32 mL of synthetic MW.

xi) Step (iii), (iv) and (v) were repeated.

xii) Beaker 5 was placed on the magnetic hotplate and spiked with 100 mL of synthetic MW.

xiii) Step (iii), (iv) and (v) were repeated.

xiv) Thereafter, turbidity of the mixture in the sample cells was measured every 5 minutes until a peak in turbidity was reached.

This described procedure was repeated for all 6 concentrations. In addition, each set of beakers was labeled in the following format: *concentration of solution – volume added*. Figure 2 shows the basic setup of the batch experiment. The entire set of experiments was then repeated in order to ensure the reproducibility of results.

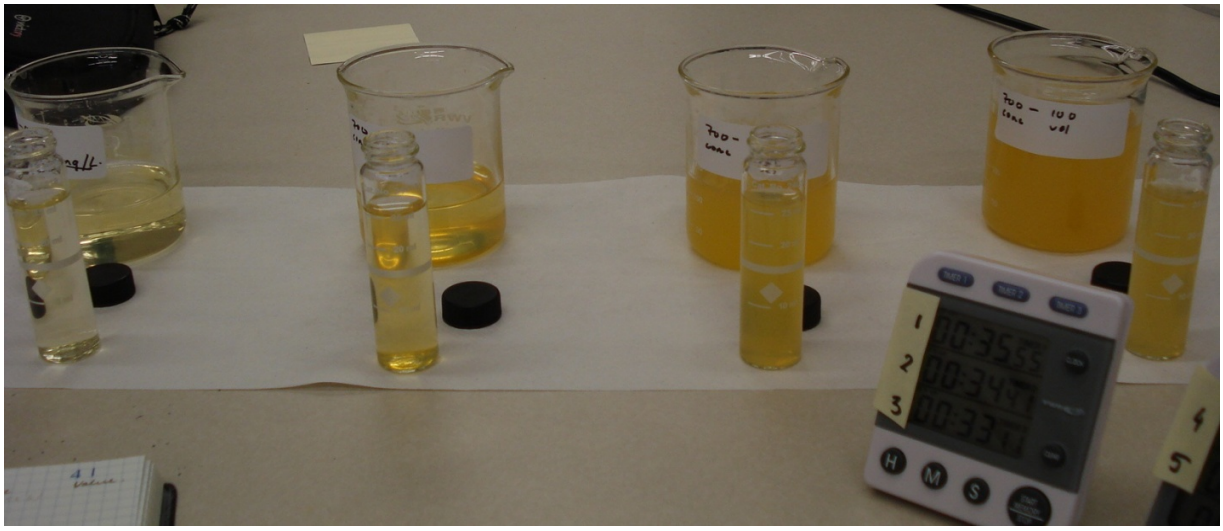

Figure 2: *Experimental setup for batch scale experiments.*

2.3 Tank experiments

The second set of experiments was conducted on a larger scale using a water tank of dimensions 0.893 m × 0.643 m × 0.320 m. Figure 3 shows an image of the tank filled with 100 L seawater.

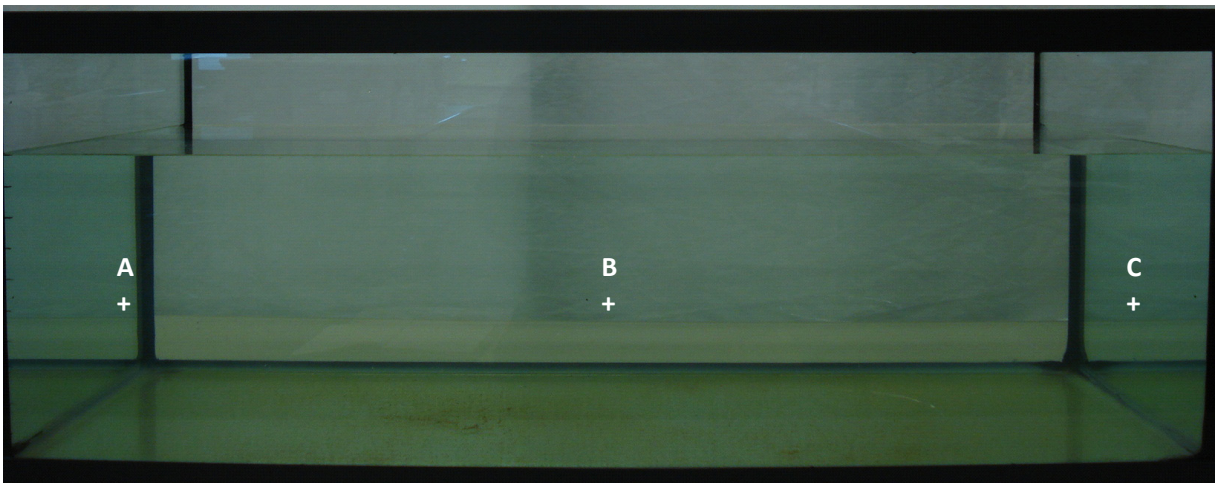

Figure 3: *Image showing the tank used with dimensions 0.893 m × 0.643 m × 0.320 m.*

Similar to the batch experiments, the tank scale involved the mixing of synthetic mine water with seawater. Here, the mixing was performed at different mixing ratios with Fe(II) concentrations of 100 mgL^{-1} and 700 mgL^{-1}. The tank was initially calibrated by filling it with 100 L seawater using a 2 L graduated cylinder and by marking it at every 10 L mark. Tank mixing experiments were performed in two different mixing ratios. Five experiments were conducted with mixing

ratio of 10 L synthetic mine water to 100 L seawater. Each of these experiments was performed at different concentrations of synthetic mine water (42.2, 100.0, 136.2, 418.1 and 678.0 mgL^{-1}). Two experiments were conducted for a mixing ratio of 50 L synthetic mine water to 50 L seawater (96.9 and 678.0 mgL^{-1}).

The following procedure was followed for each of the experiments:

i) Using a 2 L graduated cylinder, the tank was filled up to the required calibrated mark with seawater.

ii) Using a spatula and weighing balance, the exact amount of ferrous sulfate was weighed and transferred to a pre-rinsed plastic container. Table 4 shows the calculated mass of ferrous sulfate reagent used for different concentrations.

iii) The required amount (10 L or 50 L) of distilled water was added to the container. Care was taken that the water was poured down the side of the container, in order to avoid the mixing of oxygen via splashing and rapid motion.

iv) The filled container was then sealed and inverted several times to dissolve the reagent well. Rapid mixing was avoided.

v) The prepared synthetic mine water was then carefully poured into the seawater, above point B (Figure 3). Once again, care was taken to avoid water splashing out of the tank, since that would affect the oxygen content of the mixture and also the ratio of water in the tank.

vi) Once emptied, the mixture was stirred for 10 seconds with a plastic rod and then left undisturbed during the course of the measurements.

vii) 1st set of measurements was taken 5 minutes after the start of the experiment.

viii) Electrical conductivity was measured at points A, B and C using a probe attached to a HACH digital multi-meter (HQ40d Dual-Input Multi-Parameter Digital Meter).

ix) Turbidity measurements were taken at point B, using the HACH DR890 (FAU) and also with the HACH 2100P portable turbidimeter (NTU).

x) Total iron concentration was measured at point B using the HACH DR5000 UV-Vis spectrophotometer.

xi) In order to monitor occurring changes visually, digital photographs were also recorded before each set of measurements.

Table 4: *Used concentrations and corresponding added mass of $FeSO_4$ for the tank experiments.*

Fe(II), mgL^{-1}	**Volume, L**	**$FeSO_4 \cdot 7H_2O$, mg**
42.2	10	1644.7
96.9	50	24891.6
100	10	5139.6
136.2	10	4978.3
418.1	10	21490.8
678	10	34848.3
678	50	174241.4

2.3.1 Synthesizing mine water flow

In order to calculate a load based visibility limit, a third set of experiments was designed, using the same large tank scale, however by enhancing the input of mine water into the system. In order to emulate a stream-like flow, a peristaltic pump (Thermo Scientific Monostat Vera) was used to inject the synthetic mine water at a fixed pumping rate of 315 $mLmin^{-1}$. In order to ensure the synthetic mine water was injected at the water surface at all times, the outlet of the pipe was passed through a styrofoam float (Figure 4). The float was in turn, fixed on 2 plastic poles for easy movement with rising water level.

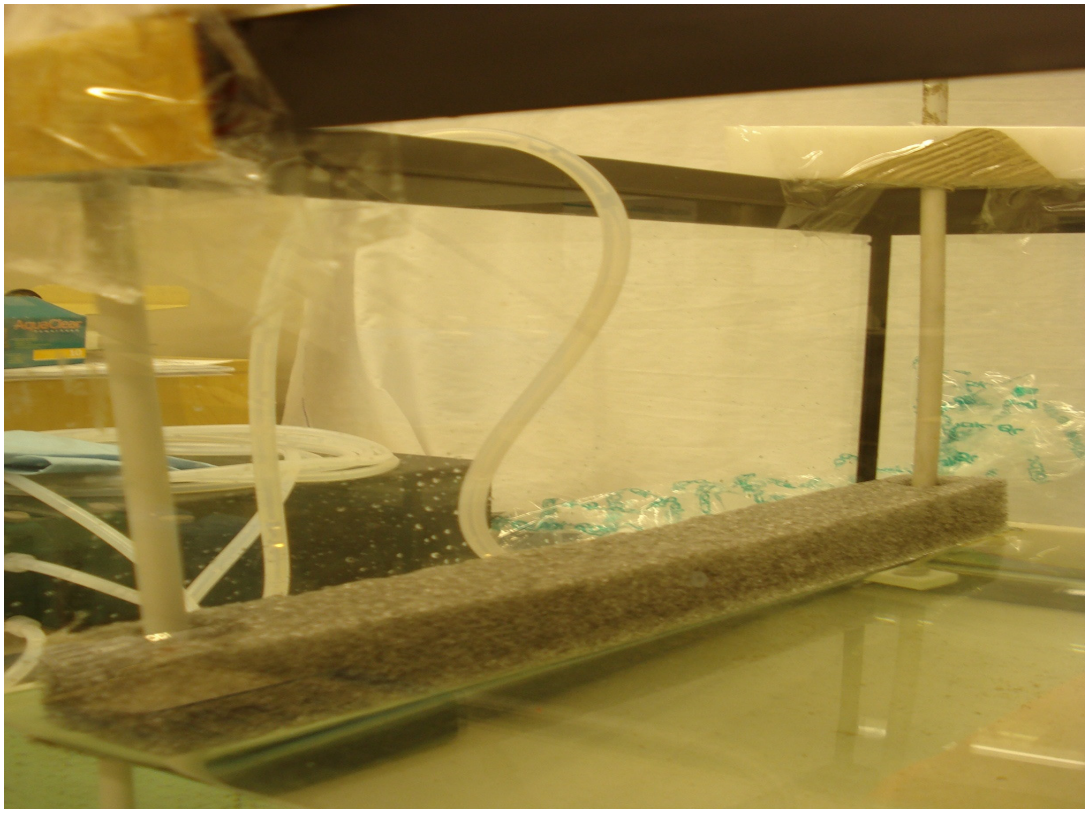

Figure 4: *Image showing the setup for load based tank experiment. The mine water outlet is fixed through a movable styrofoam float.*

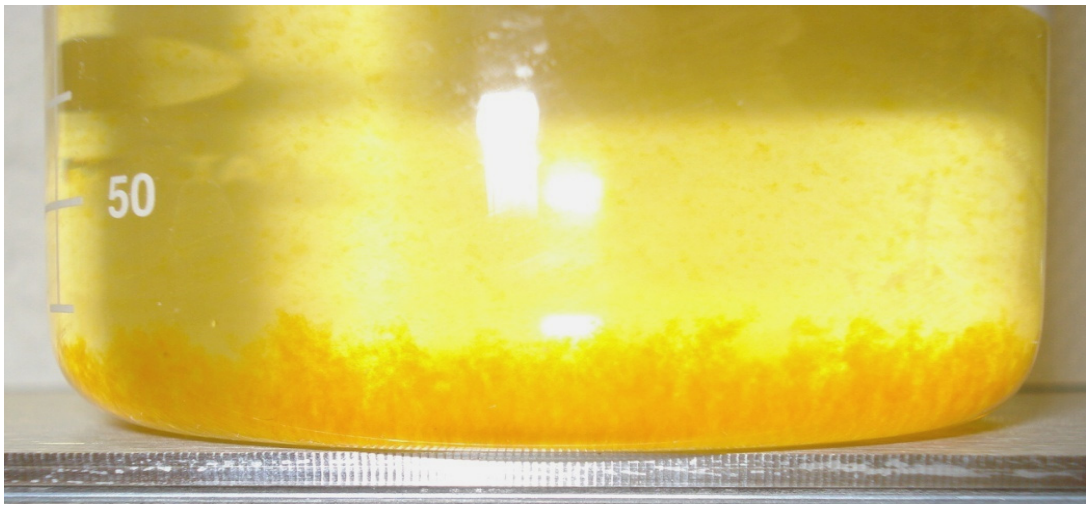

Figure 5: *Image of a beaker with Fe(II) solution and seawater mixture, showing the formation of Fe(III) precipitates at the end of experiment (after 4 hours).*

2.3.2 Synthesizing oceanic mixing

Mixing by waves is a major factor in any ocean based disposal system. For this reason, as part of the load based experiment, a well mixed scenario was setup. Mixing was simulated using the same concept as mixing in the ocean, where a constant supply of sweater is brought to shore, resulting in a dilution effect at the mine water inflow. Using a circulation pump (HAGEN™ Aqua Clear Power Head 10 Water Pump), water in the tank was pumped from point C in the direction of point A at a rate of 5 $Lmin^{-1}$. The pump was attached to the right end of the tank wall using a suction cup. Water was circulated using a plastic pipe, 50 cm in length and the pump was functional throughout the duration of the experiment.

2.4 Turbidity measurements

Turbidity is a measure of water clarity or opacity and indicates the degree to which light is scattered by suspended solids in a solution, or more specifically in this case, a mixture of two solutions (Rhoton and Bigham, 2009). Turbidity depends on a number of factors such as the size, shape color and refractive indices of the particles suspended in the solution (Hach, 2009). The turbidity that was monitored in the scope of this research was an indication of the total optical density caused by iron precipitation and flocculation. The principle units of measurement applied in these experiments were the *Formazine Attenuation Units* (FAU) and *Nephelometric Turbidity Units* (NTU). The principle behind FAU involves measurement of light that is transmitted through the sample at 180° to the line of emission. In effect, the formazine attenuation unit quantifies the decrease in transmitted light through the sample. FAU measurements were made using the HACH DR/890 portable colorimeter. The estimated detection limit is 21 FAU with a precision of ± 2 FAU. The Nephelometric method, on the other hand, involves measuring light scattered from the sample at 90° to the line of emission. NTU measurements were taken using the HACH 2100P Portable turbidimeter. This instrument provides a range of measurement between 0 and 1000 NTU with a detection limit of 0.1 NTU.

2.5 Iron measurements

Using the HACH DR890 colorimeter and the HACH DR5000 UV-Vis spectrophotometer, measurements of total iron concentration were conducted using the FerroVer Method (with powder pillows). A number of steps were followed during the measurement of total iron

concentrations using the FerroVer method. Special care was taken care that the iron is in the range of 0.02 and 3.00 mgL^{-1}. All samples with total iron > 3.00 mgL^{-1} were diluted with a measured volume of distilled water. To reach the true iron concentrations, the diluted measurements were then multiplied by the dilution factor.

The principle behind the FerroVer Method requires mixing of the FerroVer reagent with the sample. Reducing agents in the reagent reduce all except for the most resistant species of ferric (Fe(III) into the soluble ferrous (Fe(II)) state. The reduced ferrous iron in the solution then reacts with the 1-10 phenanthroline indicator to create a light orange color, the intensity of which is proportional to the concentration of total iron in the solution (Hach, 2009).

3 RESULTS AND DISCUSSION

3.1 Batch experiments

The results from the batch experiment are shown in Figures 6 to 11, which show the turbidity (FAU) change over time. Each data point indicates a single point of measurement in time. As seen from Figure 6, the turbidity values achieved for the mix of 1.4 mgL^{-1} Fe(II) solution and 100 mL seawater show very low turbidity values. This was expected as at such low ferrous iron concentrations, only minimal precipitation is possible.

In order to define a scale for the visibility of the synthetic mine water – seawater mixtures, a scale was developed based on the degree of intensity of turbidity levels. Table 5 shows the range of turbidity chosen and the visible intensity level under which fall under each range.

Table 5: *Definition of visual intensity levels based on turbidity ranges.*

Turbidity range (FAU)	Visual intensity
0 – 50	Low
50 – 150	Medium
150-250	High
> 250	Extreme

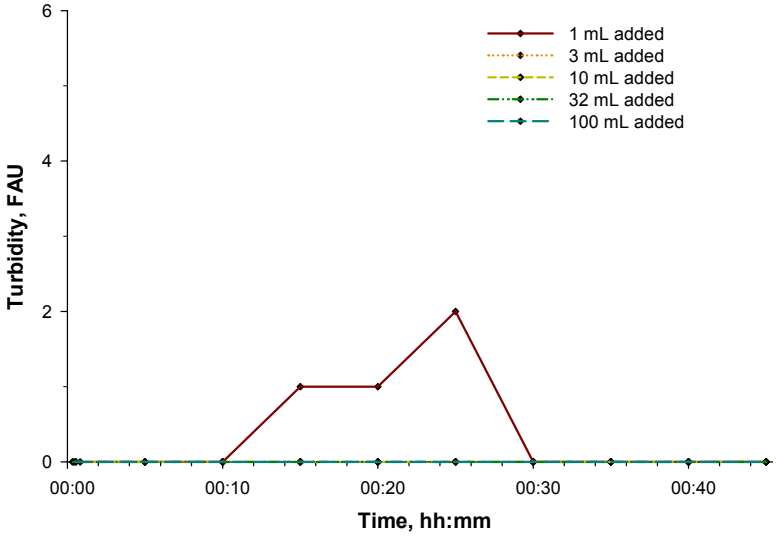

Figure 6: *Turbidity measurements for different added volumes of 1.4 mgL^{-1} Fe(II) solution to 100 mL seawater.*

In Figures 7 to 11, it can be seen that at higher iron concentrations, the range of turbidity also increases. In the mixture of added 100 mL of 13.6 mgL^{-1} Fe(II) solution and 100 mL seawater (Figure 7), the highest peak in turbidity is at approximately 40 FAU. In accordance with the definition in Table 5, 40 FAU falls under a *low* turbidity range. The observed trend is that with each increasing volume of added solution, the turbidity peaks progressively increase. This can be attributed to the fact that the more dissolved iron is present in the solution, the more precipitation occurs, leading to a higher optical density.

Another phenomenon noticed was the peaking and consequent dropping of the turbidity profiles in Figures 8 to 11. The mix of iron solution and seawater creates conditions favorable to the precipitation of Fe(III) complexes. The underlying process is the oxidation of ferrous iron, upon coming in contact with the dissolved oxygen in the seawater and the atmosphere. As the ferrous iron starts to oxidize, complexes of ferric iron begin to form. These ferric complexes, being insoluble, begin to precipitate and then flocculate, coming together and increase the turbidity of the mixture. As flocs or aggregates of ferric iron start to grow in size and volume, they accelerate the entire flocculation process, leading to larger and heavier flocs. Figure 5, shows a snapshot taken of the experiment with 100 mL (c = 136.2 mgL^{-1}) added to 100 mL seawater. In the image, precipited iron flocs at the end of the experiment (after 4 hours) can clearly be seen.

This high degree of flocculation results in the visible peak and the consequent settling of flocs results in the drop in turbidity. There are various factors that influence the mixture and chemical thermodynamics of the system. Oxygen, as mentioned before, is the primary reactant in this process. The salinity also affects the kinetics of the system.

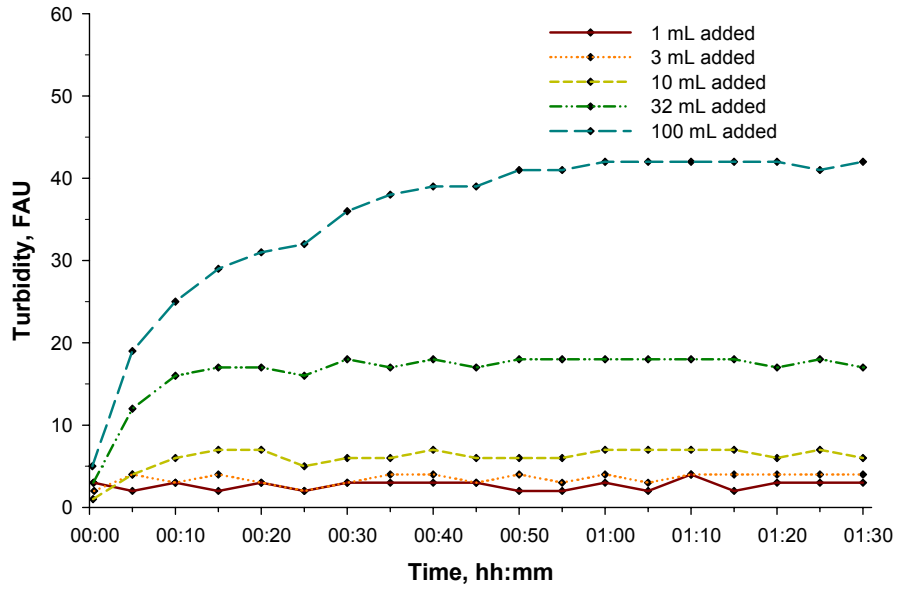

Figure 7: *Turbidity measurements for different added volumes of 13.6 mgL^{-1} Fe(II) solution to 100 mL seawater.*

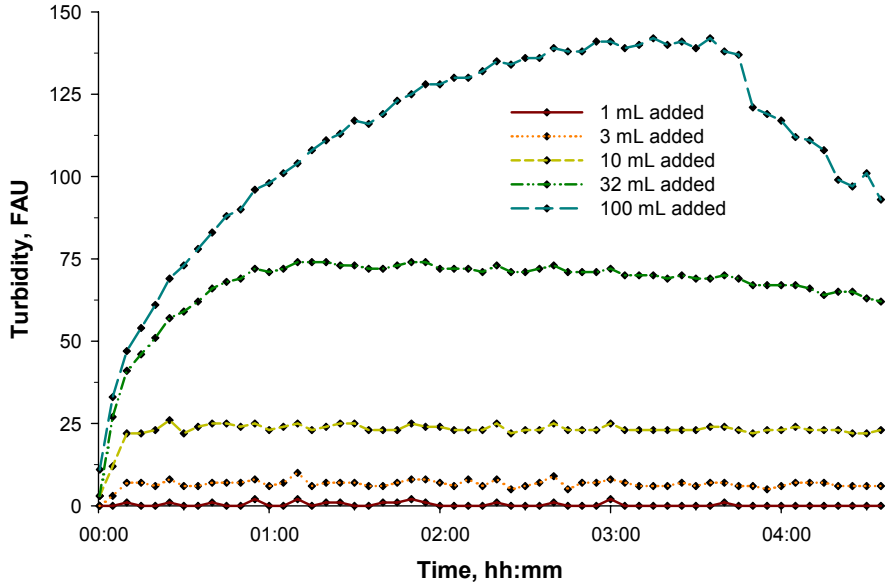

Figure 8: *Turbidity measurements for different added volumes of 43.6 mgL^{-1} Fe(II) solution to 100 mL seawater.*

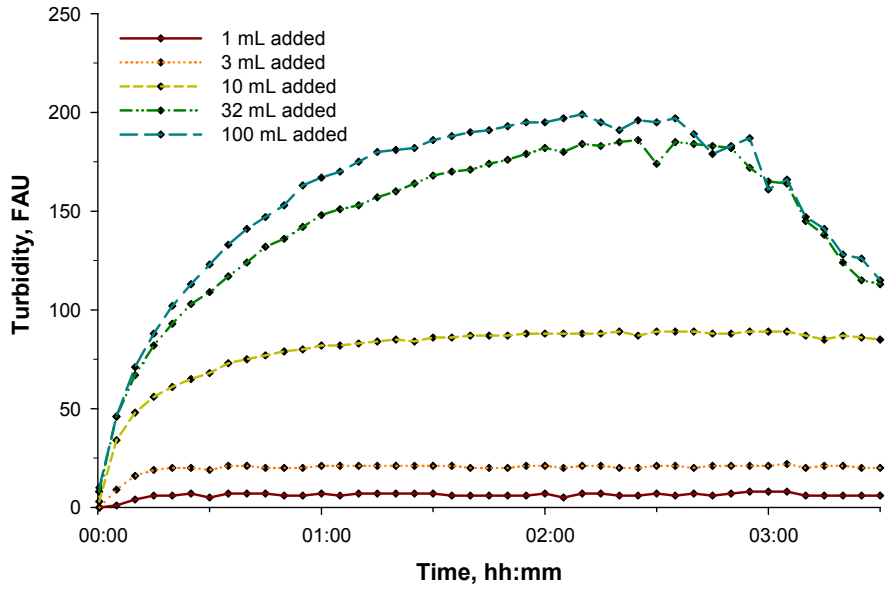

Figure 9: *Turbidity measurements for different added volumes of 136.2 mgL^{-1} Fe(II) solution to 100 mL seawater.*

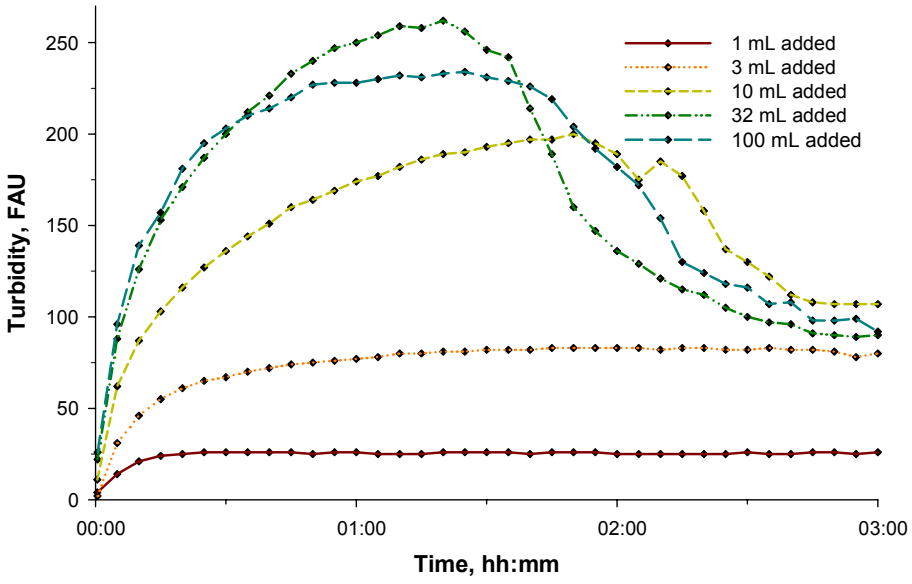

Figure 10: *Turbidity measurements for different added volumes of 431.7 mgL^{-1} Fe(II) solution to 100 mL seawater.*

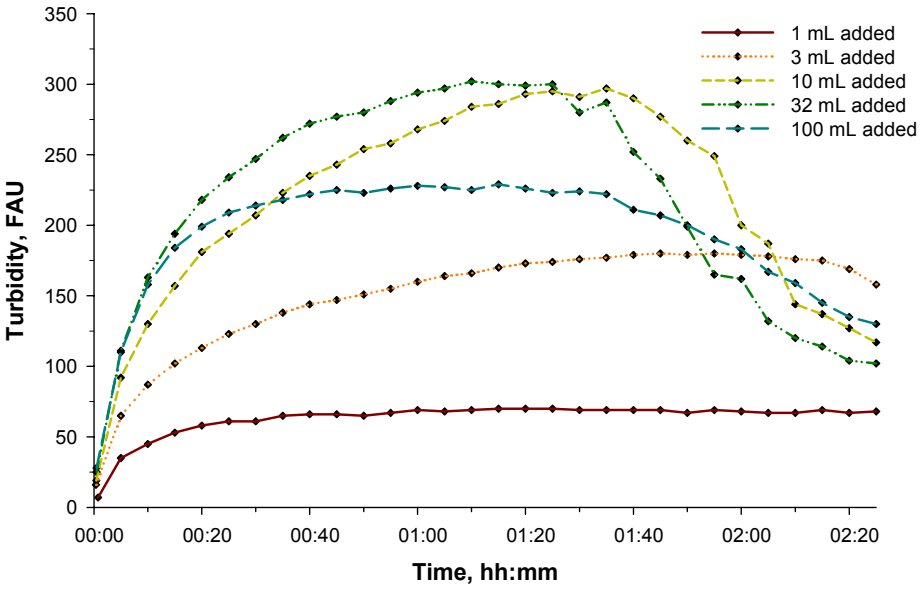

Figure 11: *Turbidity measurements for different added volumes of 953.3 mgL^{-1} Fe(II) solution to 100 mL seawater.*

In order to assess the results from a different standpoint, the results from the batch experiment were plotted a second time, with each plot representing a volume of solution added and each series indicating the Fe(II) concentration of solution added. These plots provide a better view of how a *concentration* based visibility limit could be derived (Figures 12-16).

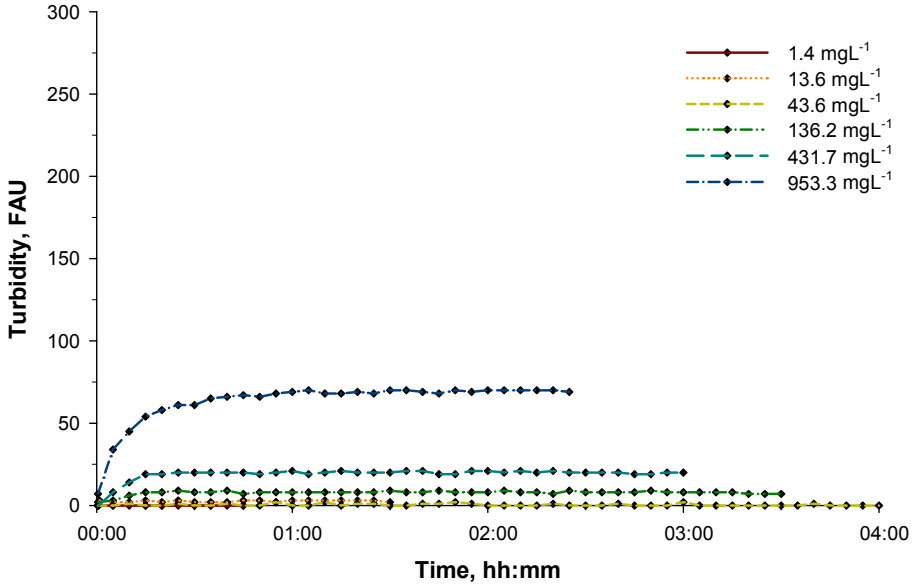

Figure 12: *Turbidity measurements for 1 mL added volume of different concentrations of Fe(II) to 100 mL seawater.*

Figure 12 shows the lowest volume (1 mL) of solution added to 100 mL seawater. All the concentrations produced turbidities in the *low* range except for 953.3 mgL^{-1}, which resulted in *medium* visual intensity (Table 5). The trend that was observed with increasing volumes can now be seen with increasing concentrations. Higher concentrations create higher turbidity. This can again be attributed to the fact that a higher concentration provides more mass of iron per unit volume, which is then subject to oxidation causing a more turbid mixture.

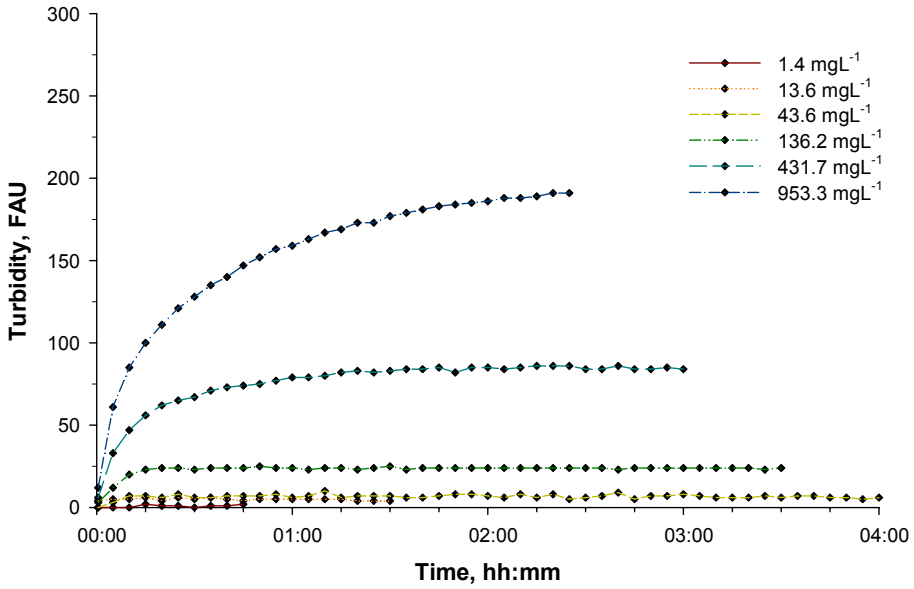

Figure 13: *Turbidity measurements for 3 mL added volume of different concentrations of Fe(II) to 100 mL seawater.*

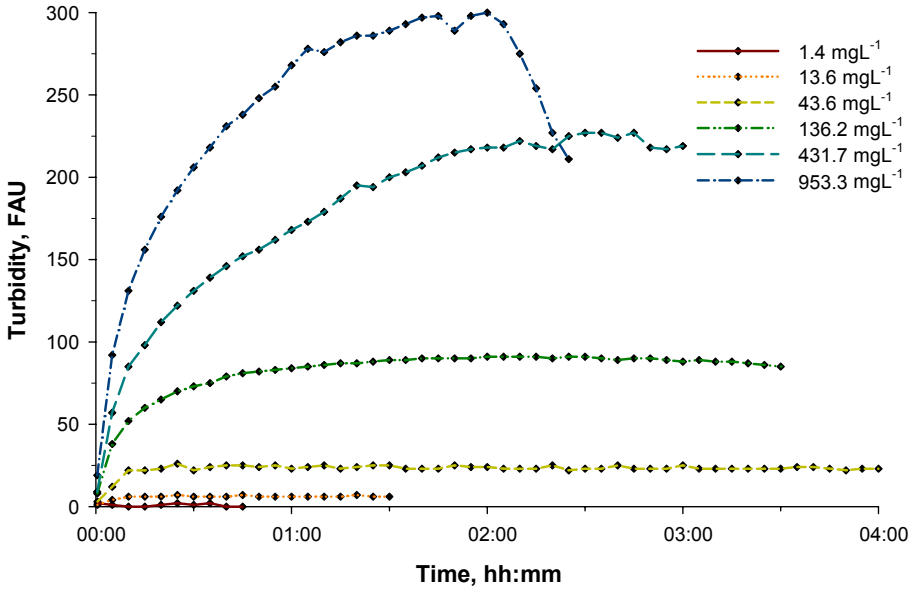

Figure 14: *Turbidity measurements for 10 mL added volume of different concentrations of Fe(II) to 100 mL seawater.*

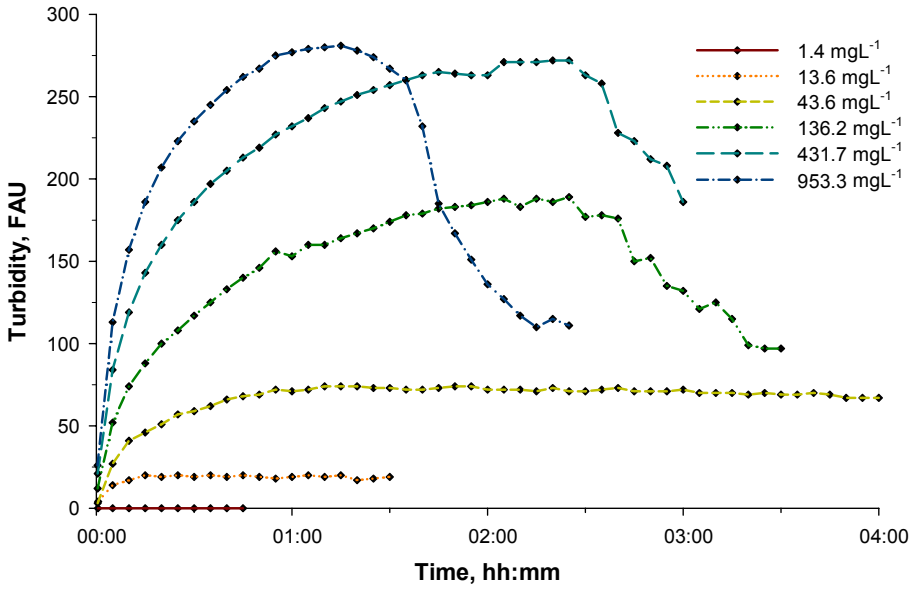

Figure 15: *Turbidity measurements for 32 mL added volume of different concentrations of Fe(II) to 100 mL seawater.*

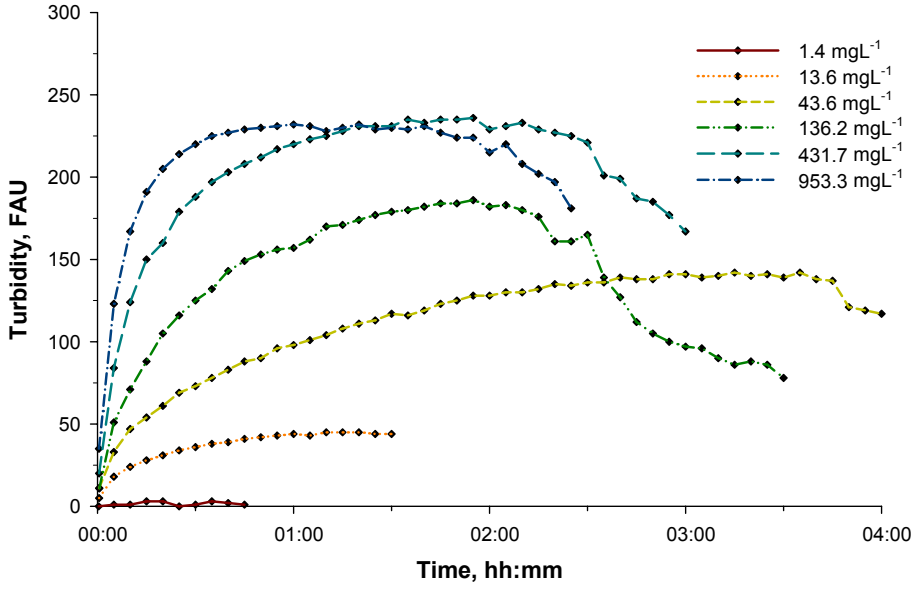

Figure 16: *Turbidity measurements for 100 mL added volume of different concentrations of Fe(II) to 100 mL seawater.*

In Figure 13, 14 and 15, the visual impact can be categorized as follows. 953.3 mgL^{-1} causes between *high* and *extreme* visibility with all volumes of solution added. 431.7 mgL^{-1} generates a visibility between *medium* and *extreme*. 136.2 mgL^{-1} shows a low visibility with 3 mL added (Figure 13), but between *medium* and *high* for consecutive larger volumes added. All other concentrations create a *low* visual impact.

It can also be seen that as the injected volumes are increased, the margin between the different turbidity levels also increases. The margin or absolute difference between the turbidity peaks for each added volume and between all concentrations is shown in Table 6. The increase in this margin is evident from the given values. The observed divergence between the series indicates that for higher concentrations ($\geq$ 136.2 mgL^{-1}) a larger volume of solution added, creates a much faster increase in the level of turbidity. It is also seen that for the peak difference between 43.6 and 136.2 mgL^{-1}, 136.2 and 431.7 mgL^{-1} and 431.7 and 953.3 mgL^{-1}, there is a volume at which there is a maximum difference, after which the difference narrows down. For example, between 136.2 and 431.7 mgL^{-1}, the turbidity margin is maximum at 10 mL added (value $\approx$ 136) and at 32 mL added, the value drops (value $\approx$ 83). This decrease in the margins is due to the onset of precipitation and settling of the oxidized iron flocs.

Table 6: *Turbidity margins between the peaks at all concentrations for each volume added to 100 mL seawater.*

Added volume mL	|FAU| between 1.4 and 13.6 mgL^{-1}	|FAU| between 13.6 and 43.6 mgL^{-1}	|FAU| between 43.56 and 136.2 mgL^{-1}	|FAU| between 136.2 and 431.7 mgL^{-1}	|FAU| between 431.7 and 953.3 mgL^{-1}
1	3	1	7	12	49
3	4	4	15	61	105
10	5	19	65	136	73
32	20	54	115	83	9
100	42	97	44	50	4

3.2 Tank experiments

3.2.1 Concentration based limit

Figure 17 shows the turbidity profiles for 10 L added to 100 L of seawater at different concentrations. The trends appear to be well correlated to the ones seen in the batch scale experiments. An increase in concentration of added solution causes an elevated degree of turbidity. The lowest concentration of 42.2 mgL^{-1} falls under the *low* visibility range whereas 100.0 mgL^{-1} and 136.2 mgL^{-1} lie at the lower end of the *medium* visibility range. The higher concentrations of 418.1 mgL^{-1} and 678.0 mgL^{-1} generate *high* and *extreme* visual impacts, respectively. With regard to the aforementioned higher concentrations, a phenomenon that is observed is the sharp dropping and consequent leveling-off of the turbidity profiles. According to (Singh et al., 1999), the initial sharp drop in the turbidity profile (after peaking) corresponds to the free settling of flocs due to gravity. With time, the degree of flocculation and the floc density in the mixture increases, leading to smaller 'inter-floc distances'. This reduction in the inter-floc distance leads to more collisions and reduced free settling, which can be seen as the leveling off or flattening of the turbidity profile.

In comparison to the batch results, Table 7 shows the peak differences between the various concentrations added. Despite the large volume of solution added (10 L) compared to a small volume (10 mL) in the batch test, the turbidity margins are very similar.

Table 7: *Turbidity margins between all concentrations for mine water to seawater mixing ratio of 1:10.*

Added volume	|FAU| between 43.6 and 136.2 mgL^{-1}	|FAU| between 136.2 and 431.7 mgL^{-1}	|FAU| between 431.7 and 953.3 mgL^{-1}
10 mL	65	136	73
10 L	50	164	67

This indicates that the change in turbidity is clearly dependant on the mixing ratio, in addition to the concentration since similar turbidity ranges were observed in the same mixing ratio (mine water **:** seawater = 10 **:** 100). This finding could help in further load based experiments, where a product of the concentration and flow rate is calculated.

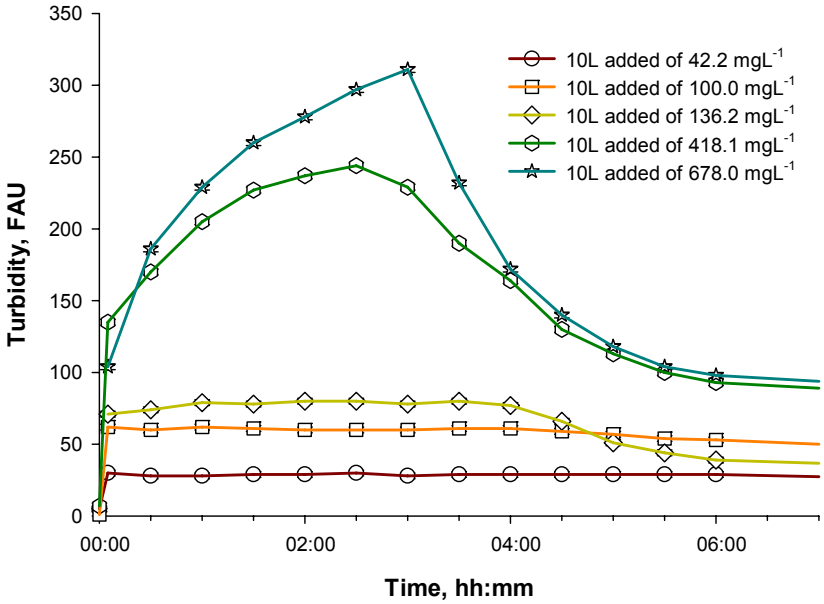

Figure 17: *Turbidity profiles at different concentrations for 10 L mine water added to 100 L seawater.*

Figure 18 shows the turbidity profiles for both 50 L and 10 L added to 50 L and 100 L of seawater, respectively. The addition of 50 L mine water to 50 L seawater tests the upper limit of feasible marine mixing of mine water, since the mixing ratio is at a maximum of 1:1. This mixing ratio does not work well from a *visibility* viewpoint. There are several reasons for this. Firstly, due to the high concentration of iron in the mixture, a high degree of turbidity is reached very rapidly. This can be seen best in the addition of 678.0 mgL^{-1}, where within 30 minutes of addition, the turbidity level went up to 256 FAU. Another important observation is that with the

1:1 mixing ratio, the turbidity of the mixture stays at a high level much longer (plateau effect) than the 1:10 mixing ratio. The iron in the mixture needs longer time to oxidize and thus precipitate due to the lower amount of oxygen (in only 50 L seawater).

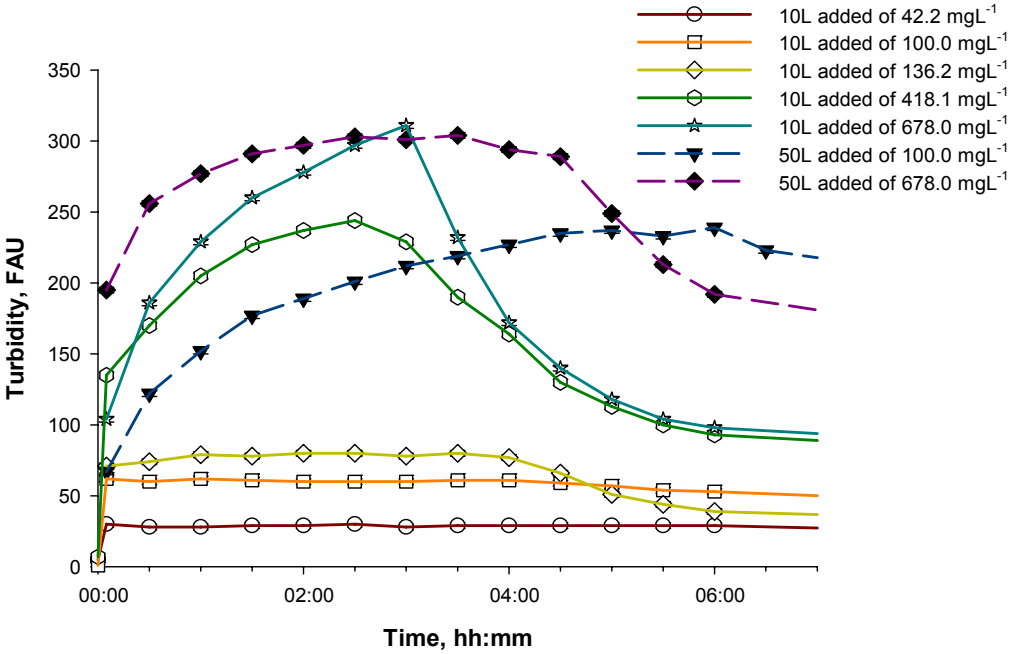

Figure 18: *Turbidity of synthetic mine water and seawater mixture at different volumes and concentrations.*

3.2.2 Stability

The stability of the mixture is also considered in the current study. A stable mixture in this respect can be defined as one which does not show fluctuation with respect to turbidity. In Figure 18, it can be seen that mixtures with 42.2 mgL^{-1}, 100.0 mgL^{-1} and partly 136.2 mgL^{-1} concentrations show a good stability. The latter however (136.2 mgL^{-1}) peaks at about 80 FAU and then starts to settle. The mixture with a concentration of 42.2 mgL^{-1} shows good stability as well except that the concentration of the mixture is fairly low. Since the aim of this work is to find a maximum visibility limit, an upper boundary must be considered. The next higher concentration that shows a good stability is 100.0 mgL^{-1}. In the context of stability, 100.0 mgL^{-1} demonstrates an upper limit for the ferrous iron concentration of a hypothetical mine water solution.

3.2.3 Visual assessment

Images taken at the measurement points corresponding to the peaks of the profiles from Figure 18 were compared with respect to color and intensity. The photographed images can be seen in Figure 19. Since the images were photographed in poor and changing light conditions (during day and night time), they are limited due to reflection, brightness/contrast and clarity imperfections. The intensifying color gradient is visible as the concentration of the added solution is increased from 42.2 mgL^{-1} to 678.0 mgL^{-1}. The mixture shown in Figure 19 a) at 42.2 mgL^{-1} is slightly semi transparent, even at peak turbidity. In contrast, the mixture Figure 19 d) shows absolute opacity with respect to light. However, in all cases, the oxidation of iron causes precipitation in varying degrees.

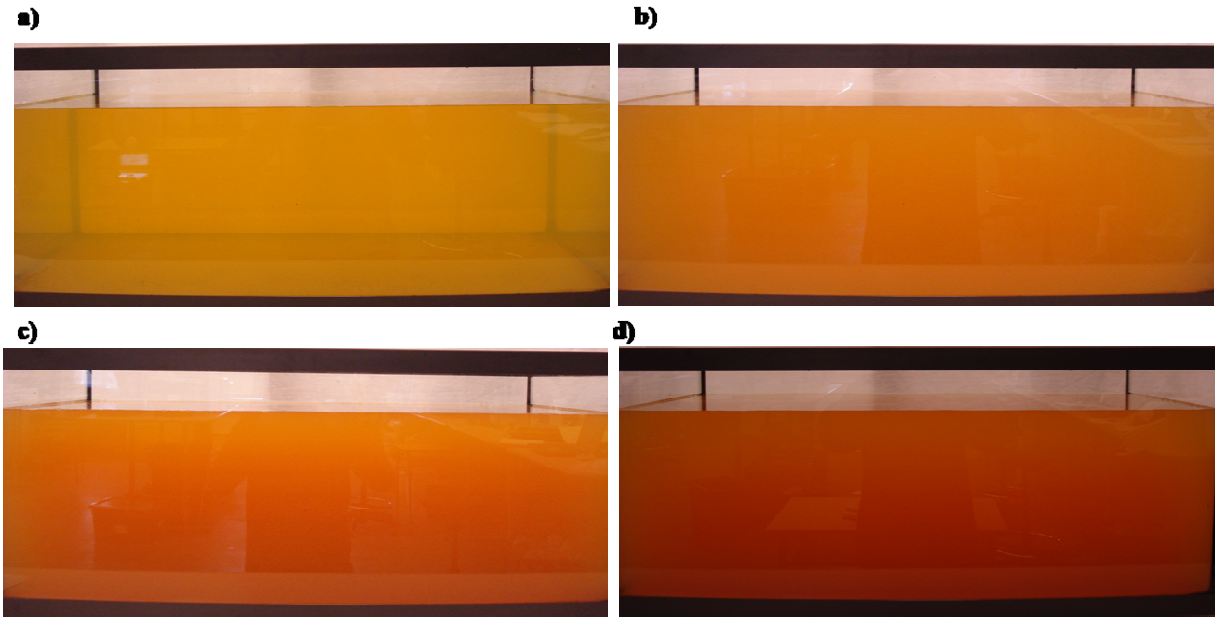

Figure 19: *Images showing the color intensity of the iron at a) 42.2 mgL^{-1}, b) 100.0 mgL^{-1}, c) 418.1 mgL^{-1} and d) 678.0 mgL^{-1} for 10 L of synthetic mine water added to 100 L seawater.*

3.2.4 Emulating mine water discharge

Load of a species is defined as its mass transported in a downstream direction, which is expressed as a rate of transport in mass per unit time (Nimick and Cleasby, 2001). This is achieved by taking the product of flow rate of the effluent stream and the concentration of the species of interest in the effluent. In order to perform a load based investigation, a concentration

of iron was selected that was postulated to be the most stable with regard to turbidity. This concentration was determined to be 100.0 mgL^{-1} (Chapter 3.2.2). Two experiments were conducted by emulating mine water flow via a peristaltic pump. 50 L of synthetic mine water (c = 100.0 mgL^{-1}) was pumped into 50 L of seawater at a flow of 0.315 $Lmin^{-1}$ (5.25×10^{-3} Ls^{-1}). This resulted in an iron loading of (5.25×10^{-3} Ls^{-1} × 100.0 mgL^{-1} = 0.525 mgs^{-1}) 45.4×10^{-3} kg/day. The first experiment integrated a mixing effect by the use of a circulation pump, whereas the second experiment was conducted without any mixing. The turbidity measurements from the experiment are shown in Figure 20. It was observed from the results that turbidity rises sharply during the pumping phase and a *high* turbidity level is achieved until the pumping stops. As soon as the 50 L of Fe solution were consumed and the pumping ceased, the turbidity increase slowed down before it started increasing again. However, with the progression of time a 'plateau' effect was created. This is similar to the effect generated by the 100 mgL^{-1} solution in the previous tank experiments (Figure 18).

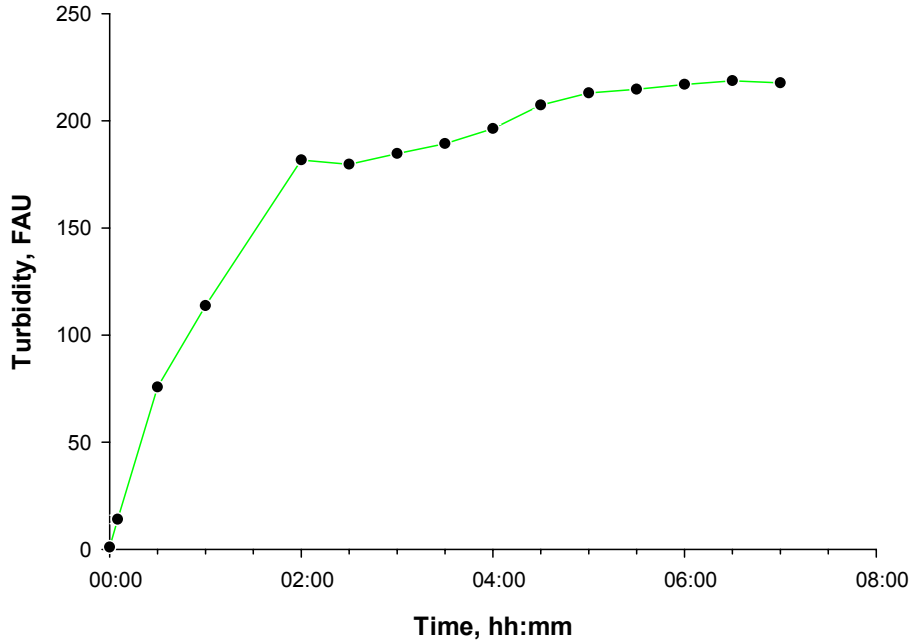

Figure 20: *Turbidity measurements for 100.0 mgL^{-1} synthetic mine water pumped into 50 L of seawater at $5.25 \times 10^{-3} Ls^{-1}$. Pumping ceased at approximately t = 02:30 hours.*

Figure 21 shows photographed images from the experiment, at every 30 minutes from the start of the experiment up to 2 hours and 30 minutes. From the photographs, the sharp increase in

turbidity can be visually assessed and as anticipated, the turbidity level increases during the pumping or discharge phase. The most dramatic change in color intensity is seen between Figure 21 a) and Figure 21 b). This color intensity corresponds to the initial sharp increase in the turbidity profile in Figure 20. From the transition between Figures 21 c), d), e) and f), it is evident that the mine water discharge leads to an increase in the overall volume of the system. In addition, a very slight change in the color intensity is also visible. Unfortunately, the photographs do not show any sharp change in the color which, can be seen well from the steep slope in the turbidity profile (Figure 20). The gradual increase in turbidity *after* the cessation of pumping could not be seen clearly by the photographs. This emphasizes the need for a better recording and a more accurate visual assessment of such a system.

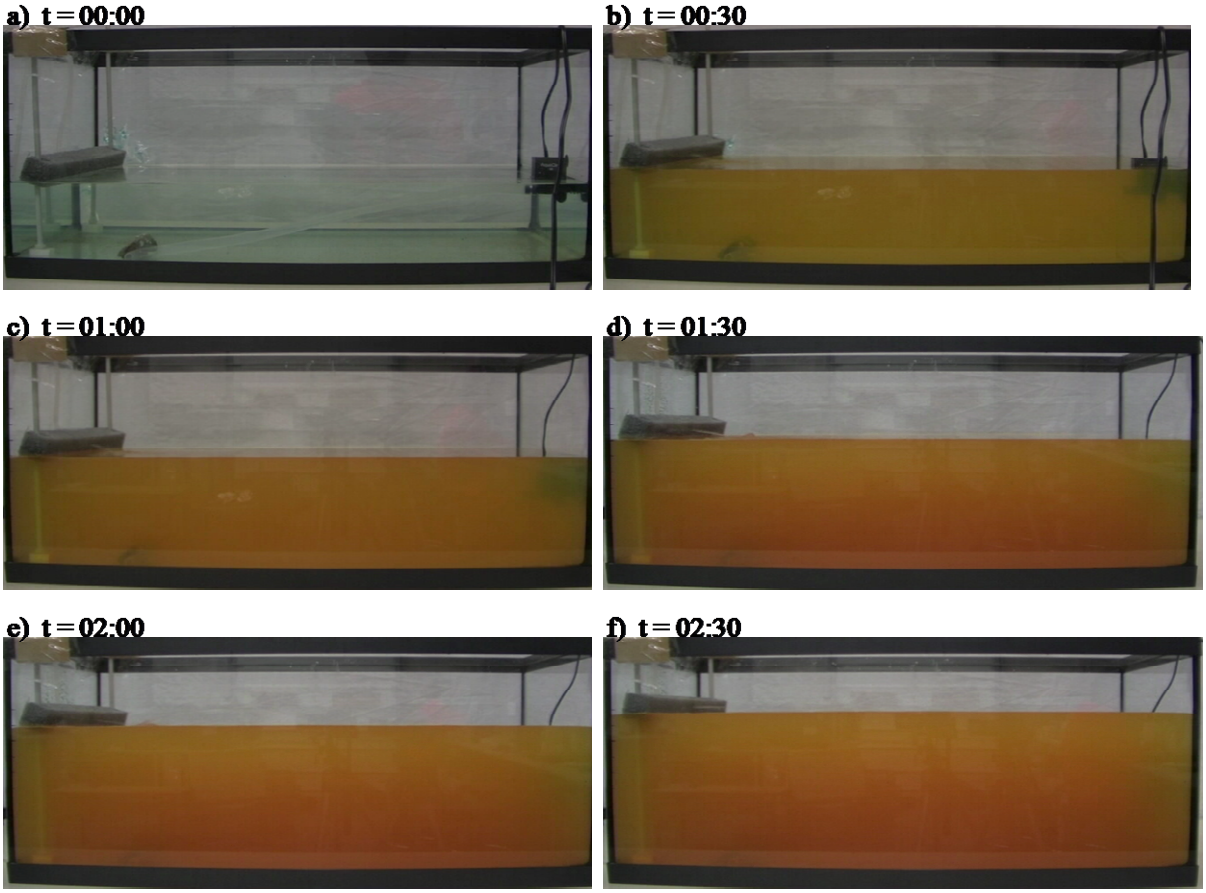

Figure 21: *Images showing color intensity from the start of the experiment up to 2:30 hours for 100.0 mgL^{-1} Fe(II) synthetic mine water discharged into 50 L seawater.*

3.3 Hydrogeochemical modeling

PHREEQC is a modeling tool for thermodynamic geochemical modeling of aquatic systems, based on the Fortran program PHREEQE (Merkel et al., 2005). In order to simulate the geochemistry of a mine water and seawater mixture, the keyword data block *mix* was implemented. This keyword simulates the mixing of 2 or more aqueous solutions. Models were generated using synthetic mine water solutions (Fe(II) solutions of different concentrations) and seawater. In order to investigate the behavior of the mixture at different mixing ratios, the model was setup in order to demonstrate the mixing of synthetic mine water and seawater in various ratios, similar to the laboratory experiments conducted.

The model was run for 1% mine water mixed with 99% seawater with an increment of 1% to the mine water at every step, up to 10%. Thereafter an increment of 5% was simulated up to 50% mine water and 50% sea water. The time at which the model was made, there was no chemical data available for a seawater sample representing the local seawaters of the Cape Breton area. Therefore a typical composition of seawater was defined as the second solution based on the PHREEQC database WATEQ4F (Ball et al., 1991). The definition of solutions and parameters used are described in Table 8.

Table 8: *Model parameters for typical seawater solution.*

Parameter	PHREEQC notation	Value
Temperature, °C	Temp	12
pH, standard units	pH	8.22
pe, no unit	pe	8.451
Density, kgL^{-1}	density	1.023
Calcium, mgL^{-1}	Ca	412.3
Magnesium, mgL^{-1}	Mg	1291.8
Sodium, mgL^{-1}	Na	10768.0
Potassium, mgL^{-1}	K	399.1
Silica (SiO_2), mgL^{-1}	Si	4.28
Chloride, mgL^{-1}	Cl	19353
Alkalinity as HCO_3^-, mgL^{-1}	Alkalinity	141.682
Sulfate as SO_4^{2-}, mgL^{-1}	S(6)	2712
Bromide, mgL^{-1}	Br	68.5

The results from the models can be seen in following figures. The species of interest included ferrous iron, ferric iron and the major species that were in equilibrium with water, specifically FeOOH (goethite), Fe_2O_3 (hematite), $FeSO_4.7H_2O$ (melanterite) and $FeCO_3$ (siderite).

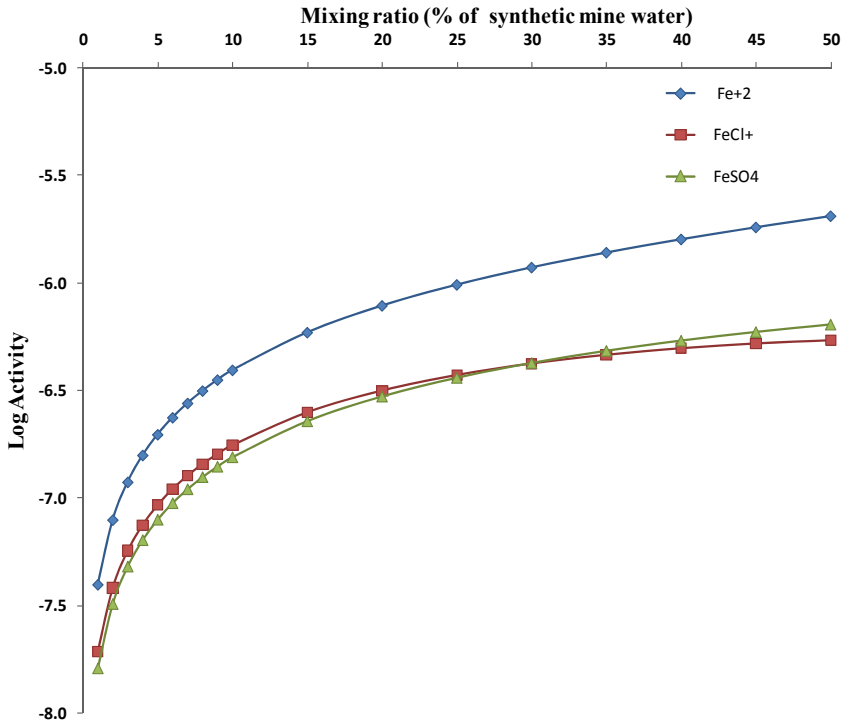

Figure 22: *Different mixing ratios (from 1% to 50% at concentration=1 mgL^{-1}) with seawater for major ferrous (Fe(II)) iron species versus log activity.*

Figure 22 shows the log activity of 3 major ferrous iron species at different mixing ratios. The *activity* of a species is a measure of its effective concentration in a solution (Langmuir, 1997). Hence as expected, with an increasing mixing ratio of synthetic mine water to seawater, the activity of the ferrous species in solution increases progressively. A time dependant model, at a fixed iron concentration would result in a steady decrease of the activities of the Fe(II) species. This is due to the fact that at a fixed concentration (when no solute is injected at a constant rate) the ferrous iron would oxidize to the ferric state. This would result in a simultaneous increase in the activities of the Fe(III) species.

The ferric iron species, as seen in Figure 23, also show an increase in activity with increased volume of added iron solution. This is again due to the oxidation of increasing Fe(II) in the mixture.

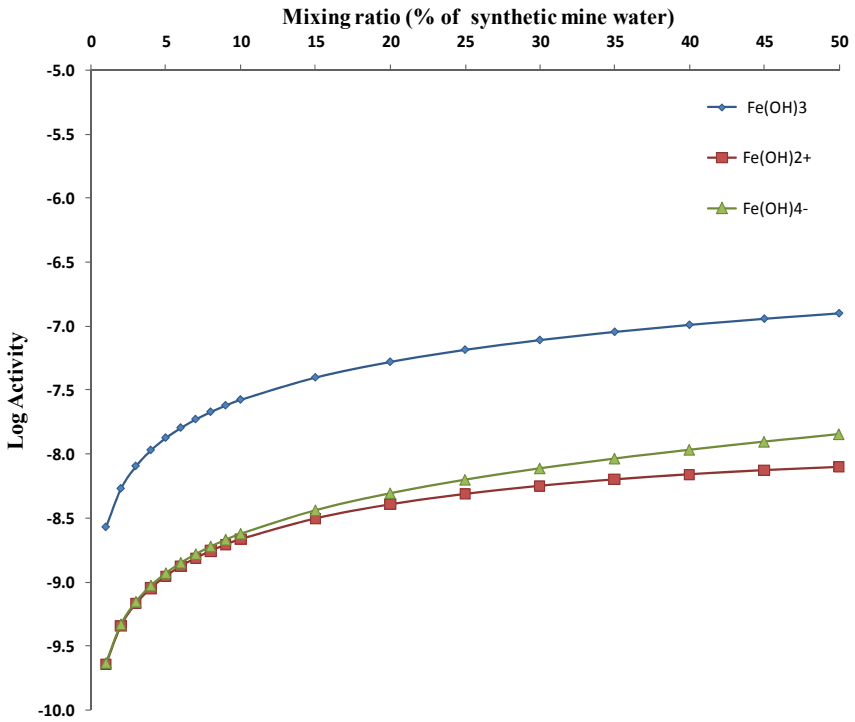

Figure 23: *Different mixing ratios (from 1% to 50% at concentration=1 mgL^{-1}) with seawater for major ferric (Fe(III)) iron species versus log activity.*

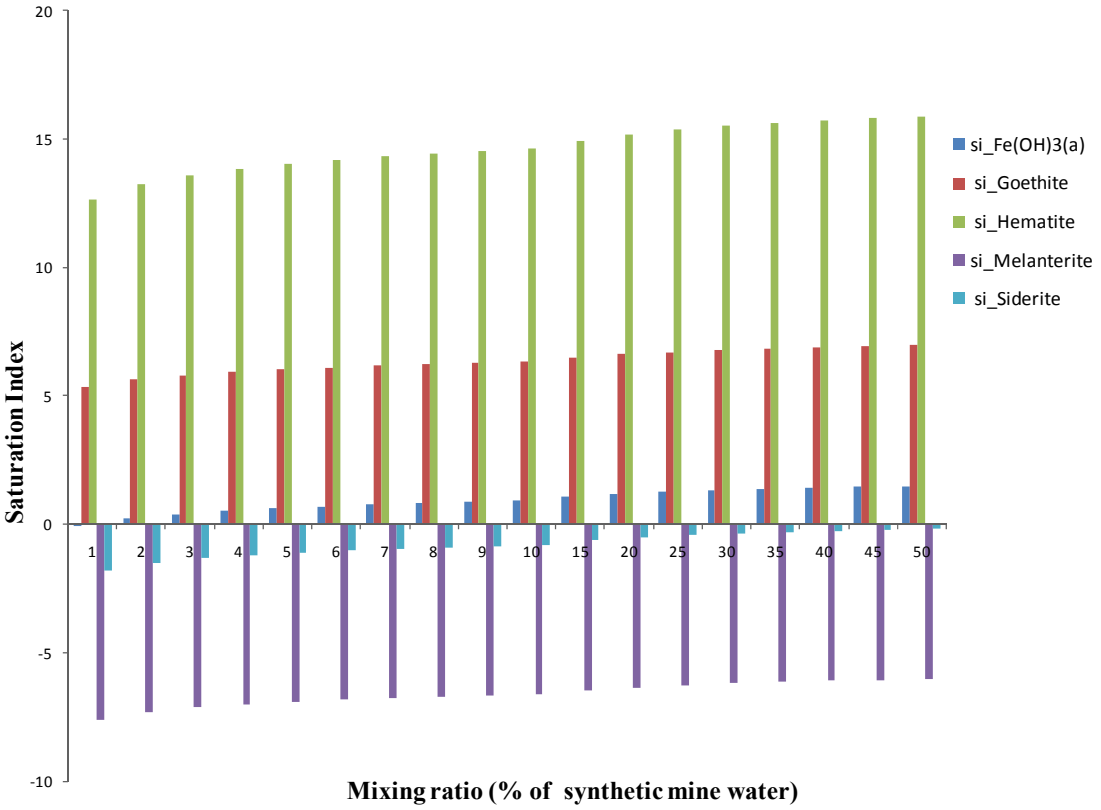

Figure 24: *Percent of mine water (conc.1mgL^{-1}) mixed with seawater versus corresponding saturation index for major Fe mineral phases.*

In Figure 24, a model was generated in order to observe the saturation indices of the major iron mineral phases in the system. The saturation indices of ferric hydroxide (amorphous), goethite, hematite, melanterite and siderite were simulated. It is evident from the figure that the saturation indices of all the mineral phases increase as the percentage of iron solution is increased in the mixture. However, it is also seen that siderite and melanterite stay under-saturated with respect to the solution mixture (negative SI) whereas $Fe(OH)_3(a)$, goethite and hematite reach saturation and then over-saturation instantly. The magnitudes of the saturation indices show that goethite is the quickest to reach an over-saturation and follows a subsequent precipitation in the mixture. The saturation indices of hematite are not representative for the current system, since hematite does not form *only* due to chemical kinetics, but its formation requires high pressure, temperature and compaction. In the formation of ochre, amorphous $Fe(OH)_3$ is produced first, which then over time gives way to form more stable phases such as goethite and jarosite (Bowell and Bruce, 1995). Due to the high ionic strength of seawater, the kinetics of Fe(II) oxidation is greatly

modified. Electrostatic interactions play a major role and affect the rate constants through ion-dipole and ion-ion interactions (Millero, 1985). However, the mineral phases responsible for the coloration of the mixture cannot be isolated since there are a number of iron-organic complexes that form alongside (Millero et al., 1987).

In order to view the mixing phenomenon at different concentrations of iron solution, models were generated for the following iron concentrations: 10 mgL^{-1}, 32 mgL^{-1}, 100 mgL^{-1}, 317 mgL^{-1} and 700 mgL^{-1}.

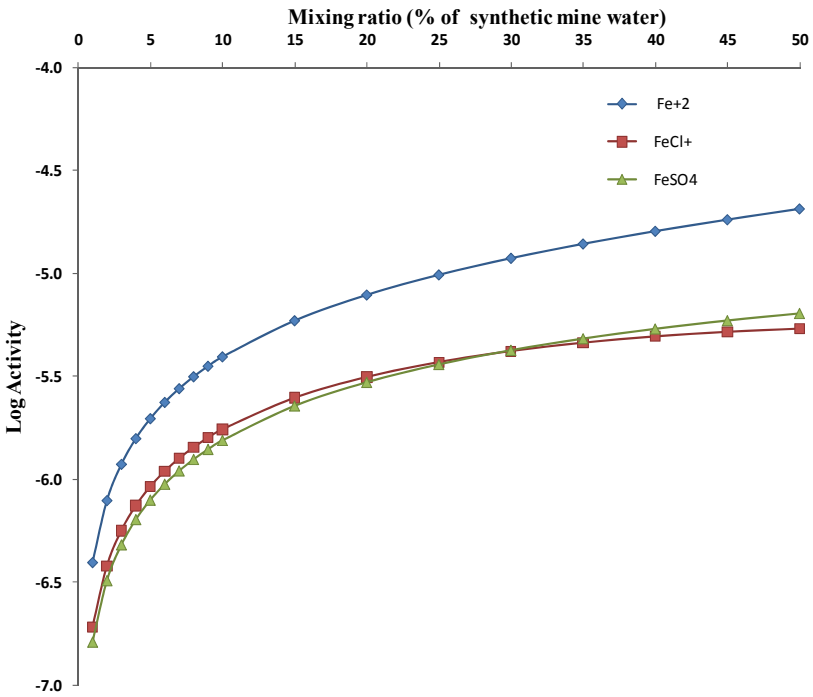

Figure 25: *Different mixing ratios (from 1% to 50% at concentration=10 mgL^{-1}) with seawater for major ferrous (Fe(II)) iron species versus log activity.*

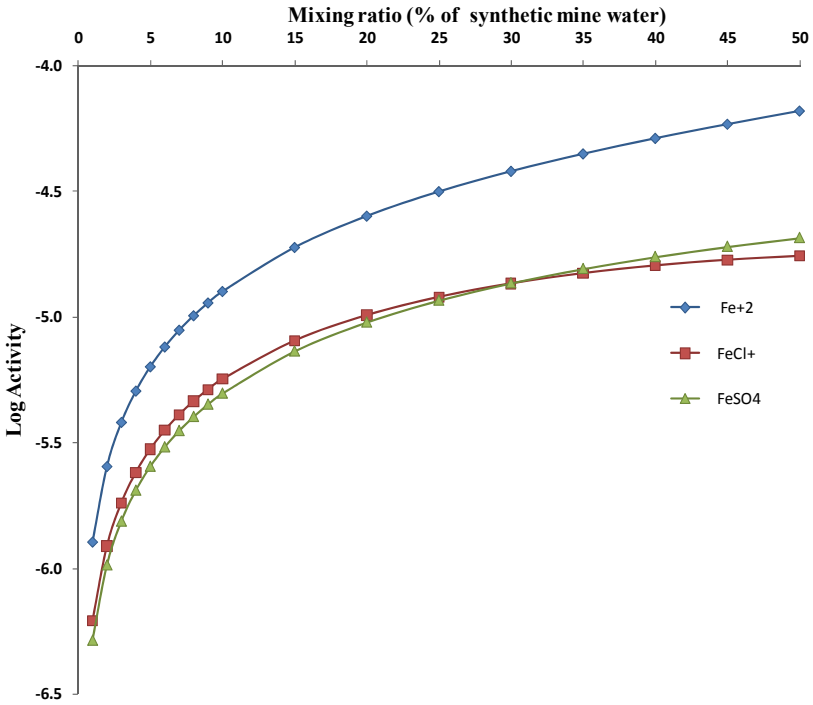

Figure 26: *Different mixing ratios (from 1% to 50% at concentration=32 mgL^{-1}) with seawater for major ferrous (Fe(II)) iron species versus log activity.*

.

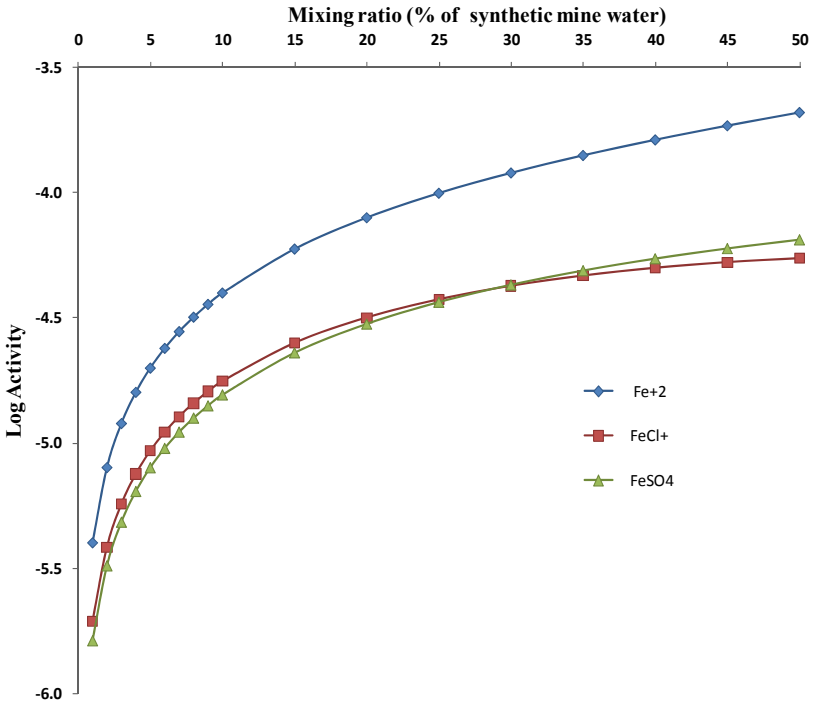

Figure 27: *Different mixing ratios (from 1% to 50% at concentration=100 mgL^{-1}) with seawater for major ferrous (Fe(II)) iron species versus log activity.*

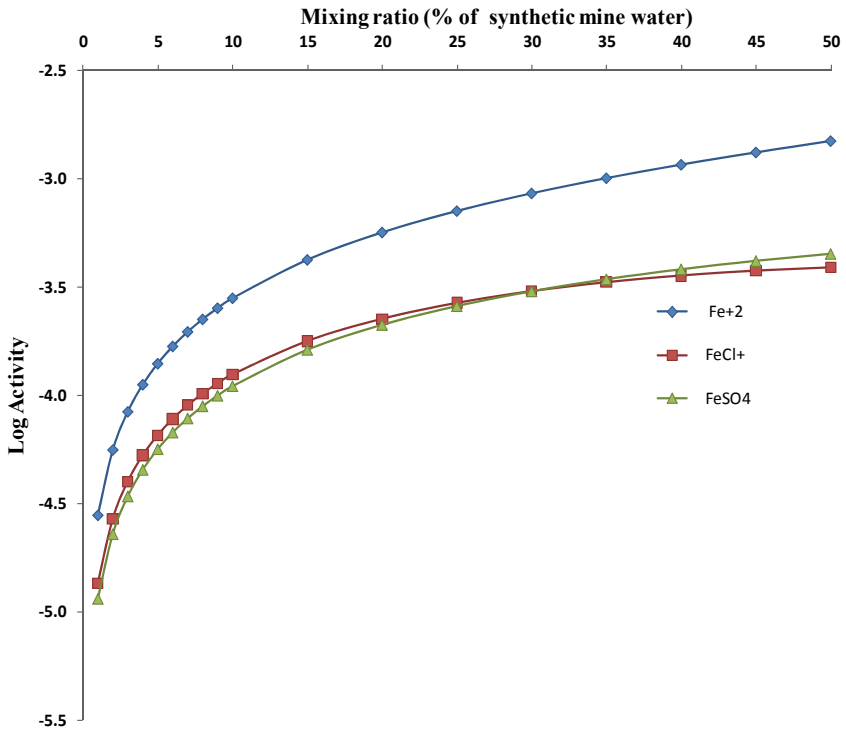

Figure 28: *Different mixing ratios (from 1% to 50% at concentration=700 mgL^{-1}) with seawater for major ferrous (Fe(II)) iron species versus log activity.*

Figures 25 to 28 show the ferrous iron activities against the mixing ratio. Comparing to Figure 22, it is evident that there is an increase in activities with concentration. A similar increase in activities was observed in the model for the ferric species. From these models, it could be postulated that the mixing of iron in seawater at different ratios is a case of conventional mixing. Although a sharp change in the activity and/or saturation index was anticipated, no such change occurred. This makes the task of determining a visibility based limit even more complex, since the mixing occurs smoothly, without any sudden or sharp chemical transformation. Considering the saturation index at different concentrations, the same phenomenon is encountered. Saturation indices of all the modeled mineral phases increase with increasing concentration. This can be observed in Figure 29.

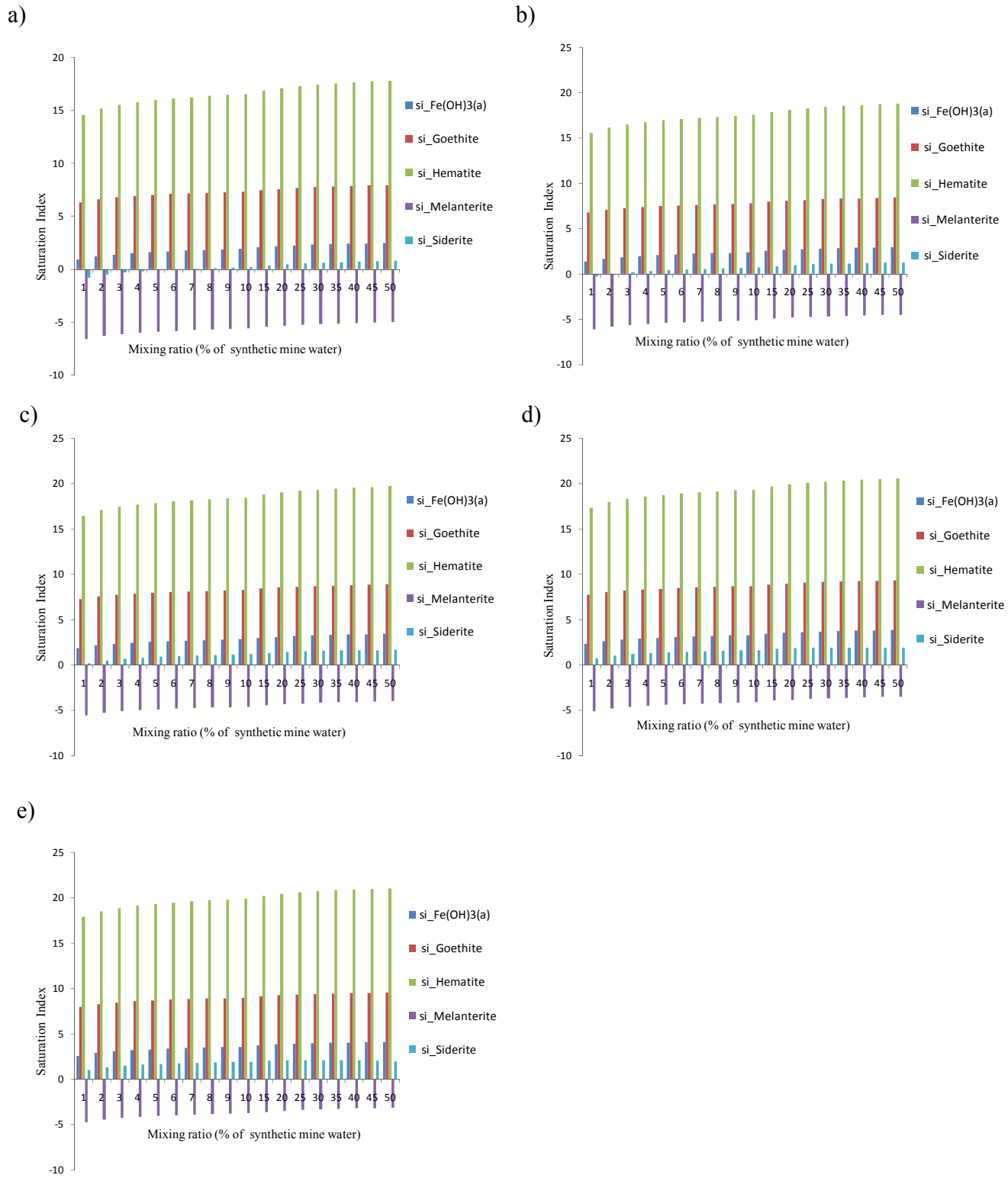

Figure 29: *Percentage of mine water added vs. saturation index (conc. 10 mgL^{-1}**(a)**, 32 mgL^{-1}**(b)**, 100 mgL^{-1}**(c)**, 317 mgL^{-1}**(d)** 700 mgL^{-1}**(e)**) for major Fe mineral phases in water.*

Models were also generated to observe the pH and oxygen concentration change in the mixture. Figure 30 shows the trends in pH over the range of mixing ratios. The increase in pH seems anomalous at first glance, since the oxidation of iron results in the generation of protons, which reduces the pH. However, it could be interpreted in terms of the alkalinity of the seawater. The pH increase seen in Figure 30 is for the lower concentrations of 1 mgL^{-1}, 10 mgL^{-1} and 32 mgL^{-1}. It could be proposed that at such low iron concentrations, the oxidation of iron does not produce enough protons to counter-act the high alkalinity of sweater and leading to a net rise in pH (Kirby et al., 2009). As the Fe concentration increases (100 mgL^{-1} and above), the alkalinity of the seawater cannot counter-act the production of protons to the same degree. This causes acidity to increase and the overall pH to drop. However, it must be mentioned here, that these changes in pH are very small and it can be suggested that more significant changes would be required before any major changes are observed in the mine water seawater mixture.

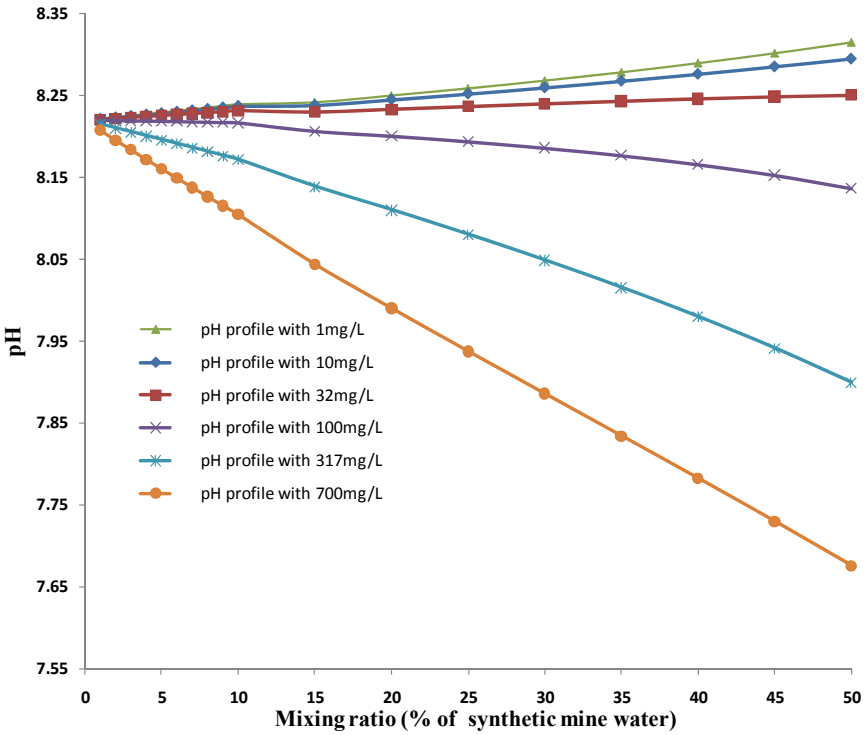

Figure 30: *Percentage of mine water mixed with seawater (in ratios from 1% to 50% at conc.1, 10, 32,100,317 and 700 mgL^{-1}) vs. pH.*

4 CONCLUSION

In an attempt to remediate one of the major aesthetically averse effects of marine disposal of mine water, this study involved performing laboratory based batch and tank scale experiments and computational modeling. The study was able to record, investigate and analyze the behavior of mine water mixing with seawater, in the context of finding a concentration and a daily load based visibility limit for the formation of red/orange iron rich ochreous plumes in the ocean.

Based on the results from the laboratory experiments and the mixing models, it can be postulated that turbidity measurements provide a good understanding for the settling of flocs and the approximate time period needed for settlement. It was observed that flocculation and then precipitation of iron occurred in solutions for all studied concentrations. This implies that in order to determine a visibility limit, one would have to select a best, approximate alternative rather than aim for total remediation of the problem.

The batch experiments revealed that with an increasing Fe concentration and volume of synthetic mine water added, turbidity of the mixture also increased. The increasing turbidity measurements suggested that the intensity of the orange/red color of iron precipitates is a time dependant and transient process. Tank experiments showed that synthetic mine water, at an Fe(II) concentration of 100 mgL^{-1} stayed very stable with regard to turbidity.

This could be recommended as an upper limit for the concentration of mine water discharge into the ocean. However, from the photographed images of the tank experiment, it can be seen that 100 mgL^{-1} (Figure 19b) generates a very dark coloration of the mixture, with high opacity. On the other hand, the next lower concentration, 42.2 mgL^{-1} (Figure 19a) displays a much lesser degree of opacity, even at peak turbidity. In addition, it is also evident that 42.2 mgL^{-1} displays good stability (Figure 18) and as discussed in chapter 3.2.1, it displays a *low* visual intensity. Therefore, in order to remain on the side of caution, an estimated concentration of 50 mgL^{-1} is proposed for discharge into the ocean.

With regard to a limit on the total iron loading, the experiments conducted were not representative of the real case scenario. This is because downscaling from the ocean scale to a tank scale is extremely complex mainly due to the scale, lack of wave mixing, temperature and

seasonal changes. However, in order to estimate a possible discharge Fe loading rate, measured field data for the flow at one of the major mine water discharges into the ocean (Cadegan Brooke) was considered here. This flow of 200 Ls^{-1} was used for the load based calculations. It was calculated that at a flow of 200 Ls^{-1} and with the proposed iron concentration of 50 mgL^{-1}, the load of Fe in kg/day would be 200 Ls^{-1} × 50 mgL^{-1} = 864 kg/day. However, this is only a recommendation and is subject to change, depending on changing flow rates or flooding events during the mine water discharge phase. When comparing our proposed limit of 864 kg Fe/day to the limit of 200 kg Fe/day suggested by Younger (2008), it is at least 4 times higher, which may seem unreasonable. However, it must be considered that in arriving at this limit, the aforementioned author did not conduct any experiments and selected it as a rough approximation, based purely on speculation. To add to that, in his paper, Younger (2008) also provides evidence of the lack of any plume associated with a 924 kg Fe/day discharge at the East Fife Coalfield, Scotland. In that context, our limit of 864 kg/day can be considered practical and applicable.

Modeling results indicate that at different mixing ratios, ferrous iron species are oxidized to generate ferric species. For all modeled concentrations (10, 32, 100, 317 and 700 mgL^{-1}) of synthetic mine water added to seawater, the activities of both the ferrous and ferric species increased in direct proportion to the ratio of mine water added to seawater. Saturation indices of the major mineral phases also followed the trend of proportional increment. In conclusion, it can be stated that the modeling results did not reveal any valuable insights and only depicted a case of conventional mixing with no sudden changes in activity or saturation index. It was also inferred that the determination of a visibility limit needs more detailed models that incorporate transport (as precipitation) and the role of organic matter so as to get a more in-depth view of the processes that control the oxidation, flocculation and subsequent precipitation of iron in seawater.

A number of errors in the measurement could be minimized or eliminated. Since most of the sampling in the experiments was done manually, there was a high degree of human error. For example, the depth from which the samples were taken for turbidity analysis was not identical for all samples. Although measurement points were defined with regard to the depth of sampling,

taking samples by hand always introduces errors in accuracy. The setup of an automatic sampling device could help in taking more accurate measurements more frequently.

In addition, various improvements could be made to the experimental setup, modeling and sampling protocols pertaining to this study.

- Large scale tank experiments must be conducted which investigate the stability and color intensity of synthetic mine water solutions of Fe(II) concentrations lower than 50 mgL^{-1}, in order to set a possibly lower limit on the discharge concentration of iron.
- In any attempt to simulate the dynamics of the ocean in the laboratory, there are still factors that are not considered yet. The dilution factor of the ocean is considered infinite and this will always be a challenge to simulate in the laboratory. However, performing the experiments on an even larger scale (than the one performed in this study) will help in taking into account this factor.
- The mixing action of waves in the ocean is another important factor that could be integrated in future experiments. This is because wave action not only creates motion and physical mixing, but it also creates a constant supply of freshly oxygenated water to the reactions.
- With regard to assessing a visual effect, a better photography and/or recording system should be utilized, with appropriate filters that negate the effects of reflecting light and 'visual noise'.
- In connection to the mine water disposal site and from a management standpoint, precaution is always the most feasible option, even before remediation. Hence, a monitoring station with a treatment system should be setup at the point where the mine water is discharged into the ocean. This way, a loading rate below the recommended Fe discharge load of 864 kg/day can be maintained, as a precautionary measure.

References

Ball, J. W., Nordstrom, D. K. & Geological Survey (U.S.) 1991. *User's manual for WATEQ4F, with revised thermodynamic data base and text cases for calculating speciation of major, trace, and redox elements in natural waters.* 2.0. ed.: U.S. Geological Survey.

Banks, S. B. & Banks, D. 2001. Abandoned mines drainage: impact assessment and mitigation of discharges from coal mines in the UK. *Engineering Geology,* 60**,** 31-37.

Bowell, R. J. & Bruce, I. 1995. Geochemistry of iron ochres and mine waters from Levant Mine, Cornwall. *Applied Geochemistry,* 10**,** 237-250.

Boyle, E. A., Edmond, J. M. & Sholkovitz, E. R. 1977. The mechanism of iron removal in estuaries. *Geochimica et Cosmochimica Acta,* 41**,** 1313-1324.

Davies, G., Butler, D., Mills, M. & Williams, D. 1997. A Survey of Ferruginous Minewater Impacts in the Welsh Coalfields. *Water and Environment Journal,* 11**,** 140-146.

Gray, N. F. 1996. A substrate classification index for the visual assessment of the impact of acid mine drainage in lotic systems. *Water Research,* 30**,** 1551-1554.

Hach 2009. *DR/890 Colorimeter Procedures Manual.*, Hach Company.

Jarvis, A. P. & Younger, P. L. 2000. Broadening the scope of mine water environmental impact assessment: a UK perspective. *Environmental Impact Assessment Review,* 20**,** 85-96.

Kirby, C. S. & Brady, J. A. E. 1998. Field determination of Fe2+ oxidation rates in acid mine drainage using a continuously-stirred tank reactor. *Applied Geochemistry,* 13**,** 509-520.

Kirby, C. S., Dennis, A. & Kahler, A. 2009. Aeration to degas CO2, increase pH, and increase iron oxidation rates for efficient treatment of net alkaline mine drainage. *Applied Geochemistry,* 24**,** 1175-1184.

Langmuir, D. 1997. *Aqueous environmental geochemistry,* Upper Saddle River, N.J., Prentice Hall.

Lewin, J. & Chen, C. H. 1973. Changes in the concentration of soluble and particulate iron in sea water enclosed in containers. *Limnology and Oceanography,* 18**,** 590-596.

Liu, X. & Millero, F. J. 2002. The solubility of iron in seawater. *Marine Chemistry,* 77**,** 43-54.

Merkel, B. J., Planer-Friedrich, B. & Nordstrom, D. K. 2005. *Groundwater Geochemistry: A Practical Guide to Modeling of Natural and Contaminated Aquatic Systems.* Berlin, Heidelberg: Springer-Verlag Berlin Heidelberg.

Millero, F. J. 1985. The effect of ionic interactions on the oxidation of metals in natural waters. *Geochimica et Cosmochimica Acta,* 49**,** 547-553.

Millero, F. J., Sotolongo, S. & Izaguirre, M. 1987. The oxidation kinetics of Fe(II) in seawater. *Geochimica et Cosmochimica Acta,* 51**,** 793-801.

Nimick, D. A. & Cleasby, T. E. 2001. Quantification of metal loads by tracer injection and synoptic sampling in Daisy Creek and the Stillwater River, Park County, Montana, August 1999. *USGS Water-Resources Investigations Report 00-4261.*

Rhoton, F. E. & Bigham, J. M. 2009. Natural Ferrihydrite as an Agent for Reducing Turbidity Caused by Suspended Clays. *J Environ Qual,* 38**,** 1887-1891.

Roekens, E. J. & Van Grieken, R. 1983. Kinetics of iron(II) oxidation in seawater of various pH. *Marine Chemistry,* 13**,** 195-202.

Shea, J. 2008. Innovative mine water management techniques for submarine coal mines of the Sydney Coalfield, Nova Scotia. *Proceedings of the West Virginia mine drainage task force symposium.* Morgantown, West Virginia. .

Sholkovitz, E. R. 1976. Flocculation of dissolved organic and inorganic matter during the mixing of river water and seawater. *Geochimica et Cosmochimica Acta,* 40**,** 831-845.

Singh, B. P., Besra, L. & Prasad, A. R. 1999. Coagulation and flocculation study of iron ore fines. *Separation Science and Technology,* 34**,** 743 - 753.

Somerfield, P. J., Michael Gee, J. & Warwick, R. M. 1994. Benthic community structure in relation to an instantaneous discharge of waste water from a tin mine. *Marine Pollution Bulletin,* 28**,** 363-369.

Tiwary, R. K. 2001. Environmental impact of coal mining on water regime and its management. *Water, Air, & Soil Pollution,* 132**,** 185-199.

Watten, B. J., Sibrell, P. L. & Schwartz, M. F. 2005. Acid neutralization within limestone sand reactors receiving coal mine drainage. *Environmental Pollution,* 137**,** 295-304.

Wolkersdorfer, C. 2002. Mine water tracing. *Geological Society, London, Special Publications,* 198**,** 47-60.

Wolkersdorfer, C. 2008. *Water Management at Abandoned Flooded Underground Mines: Fundamentals, Tracer Tests, Modelling, Water Treatment.* Berlin, Heidelberg: Springer-Verlag Berlin Heidelberg.

Wood, S. C., Younger, P. L. & Robins, N. S. 1999. Long-term changes in the quality of polluted minewater discharges from abandoned underground coal workings in Scotland. *Quarterly Journal of Engineering Geology and Hydrogeology,* 32**,** 69-79.

Younger, P. 2008. Towards Regulatory Criteria for Discharging Iron-rich Mine Water into the Sea. *Mine Water and the Environment,* 27**,** 56-61.

Younger, P. L., Banwart, S. A. & Hedin, R. S. 2002. *Mine water : hydrology, pollution, remediation,* Dordrecht ; Boston, Kluwer Academic Publishers.

Appendix

1. PHREEQC code:

```
TITLE MDC Mixing Sea Water with Synthetic Mine Water

PRINT  #this controls which of the commands are active and which are
inactive.
-reset true
-saturation_indices  true
-selected_output     true
-species             true


SOLUTION 1 Synthetic Mine Water 100mg/L Fe
    temp      15
    pH        6.5
    pe        4.5
    redox     pe
    units     mg/l
    density   1
    Fe        100
    -water    1 # kg
SAVE solution 1
END


SOLUTION 2 Synthetic Mine Water 700mg/L Fe
    temp      15
    pH        6.5
    pe        4.5
    redox     pe
    units     mg/l
    density   1
    Fe        700
    -water    1 # kg
SAVE solution 2
END


TITLE Definition of seawater.
SOLUTION 3 Seawater
    temp      12
    pH        8.22
    pe        8.451
    redox     pe
    units     ppm
    density   1.023
    Ca        412.3
    Mg        1291.8
    Na        10768
    K         399.1
    Si        4.28
    Cl        19353
```

```
    Alkalinity 141.682 as HCO3
    S(6)      2712
    Br        68.5
    -water    1 # kg
SAVE solution 3
END

SELECTED_OUTPUT
-file SI_700mg_L.sel
-selected_out    true
-user_punch      true
-activities Fe+2 FeCl+ FeSO4 FeHCO3+ FeCO3 FeOH+ Fe(OH)2 Fe(OH)3-
-activities FeHSO4+ Fe(HS)2 Fe(HS)3- Fe(OH)3 Fe(OH)2+ Fe(OH)4- FeOH+2
-activities FeSO4+ FeCl+2 FeCl2+ Fe+3 Fe(SO4)2- FeCl3 Fe2(OH)2+4
-activities Fe3(OH)4+5 FeHSO4+2
-saturation_indices Fe(OH)3(a) Goethite Hematite Jarosite-K
-saturation_indices Melanterite Siderite

-activities O2

TITLE Mix x% 1 mg/L mine water with seawater at
x=1,2,...10,15,20,25,30,...45,50 %.

MIX 1
       2     0.01
       3      0.99
SAVE solution   4
END

MIX 2
       2     0.02
       3      0.98
SAVE solution   5
END

MIX 3
       2     0.03
       3      0.97
SAVE solution   6
END

MIX 4
       2     0.04
       3      0.96
SAVE solution   7
END

MIX 5
       2     0.05
       3      0.95
SAVE solution   8
END

MIX 6
       2     0.06
       3      0.94
```

```
SAVE solution   9
END

MIX 7
       2     0.07
       3      0.93
SAVE solution   10
END

MIX 8
       2     0.08
       3      0.92
SAVE solution   11
END

MIX 9
       2     0.09
       3      0.91
SAVE solution   12
END

MIX 10
       2     0.10
       3      0.90
SAVE solution   13
END

MIX 11
       2     0.15
       3      0.85
SAVE solution   14
END

MIX 12
       2     0.20
       3      0.80
SAVE solution   15
END

MIX 13
       2     0.25
       3      0.75
SAVE solution   16
END

MIX 14
       2     0.30
       3      0.70
SAVE solution   17
END

MIX 15
       2     0.35
       3      0.65
SAVE solution   18
END
```

```
MIX 16
       2      0.40
       3       0.60
SAVE solution   19
END

MIX 17
       2      0.45
       3       0.55
SAVE solution   20
END

MIX 18
       2      0.50
       3       0.50
SAVE solution   21
END
```

2. Turbidity measurements for batch experiments:

Note: Each column represents the time and the corresponding turbidity measurements (FAU) in the format of *concentration – volume*. For example, a column heading: *Turbidity 001-003* stands for turbidity measurements for 1 mgL^{-1} Fe(II) of synthetic mine water and 3 mL of added volume.

1-Time_001-001	2-Turbidity_001-001	3-Time_001-003	4-Turbidity_001-003	5-Time_001-010	6-Turbidity_001-010	7-Time_001-032	8-Turbidity_001-032	9-Time_001-100	10-Turbidity_001-100
00:00:23	0.0000	00:00:25	0.0000	00:00:37	2.0000	00:00:32	0.0000	00:00:23	0.0000
00:05:00	0.0000	00:05:00	0.0000	00:05:00	1.0000	00:05:00	0.0000	00:05:00	1.0000
00:10:00	0.0000	00:10:00	0.0000	00:10:00	0.0000	00:10:00	0.0000	00:10:00	1.0000
00:15:00	0.0000	00:15:00	2.0000	00:15:00	0.0000	00:15:00	0.0000	00:15:00	3.0000
00:20:00	0.0000	00:20:00	1.0000	00:20:00	1.0000	00:20:00	0.0000	00:20:00	3.0000
00:25:00	0.0000	00:25:00	1.0000	00:25:00	2.0000	00:25:00	0.0000	00:25:00	0.0000
00:30:00	0.0000	00:30:00	0.0000	00:30:00	1.0000	00:30:00	0.0000	00:30:00	1.0000
00:35:00	0.0000	00:35:00	1.0000	00:35:00	2.0000	00:35:00	0.0000	00:35:00	3.0000
00:40:00	0.0000	00:40:00	1.0000	00:40:00	0.0000	00:40:00	0.0000	00:40:00	2.0000
00:45:00	0.0000	00:45:00	2.0000	00:45:00	0.0000	00:45:00	0.0000	00:45:00	1.0000

12-Time_010-001	13-Turbidity_010-001	14-Time_010-003	15-Turbidity_010-003	16-Time_010-010	17-Turbidity_010-010	18-Time_010-032	19-Turbidity_010-032	20-Time_010-100	21-Turbidity_010-100
00:00:52	3.0000	00:00:25	4.0000	00:00:30	1.0000	00:00:35	4.0000	00:00:29	5.0000
00:05:00	2.0000	00:05:00	5.0000	00:05:00	4.0000	00:05:00	14.0000	00:05:00	18.0000
00:10:00	2.0000	00:10:00	5.0000	00:10:00	6.0000	00:10:00	17.0000	00:10:00	24.0000
00:15:00	3.0000	00:15:00	6.0000	00:15:00	6.0000	00:15:00	20.0000	00:15:00	28.0000
00:20:00	2.0000	00:20:00	4.0000	00:20:00	6.0000	00:20:00	19.0000	00:20:00	31.0000
00:25:00	3.0000	00:25:00	6.0000	00:25:00	7.0000	00:25:00	20.0000	00:25:00	34.0000
00:30:00	2.0000	00:30:00	5.0000	00:30:00	6.0000	00:30:00	19.0000	00:30:00	36.0000
00:35:00	2.0000	00:35:00	6.0000	00:35:00	6.0000	00:35:00	20.0000	00:35:00	38.0000
00:40:00	2.0000	00:40:00	5.0000	00:40:00	6.0000	00:40:00	19.0000	00:40:00	39.0000
00:45:00	3.0000	00:45:00	4.0000	00:45:00	7.0000	00:45:00	20.0000	00:45:00	41.0000
00:50:00	3.0000	00:50:00	5.0000	00:50:00	6.0000	00:50:00	19.0000	00:50:00	42.0000
00:55:00	2.0000	00:55:00	5.0000	00:55:00	6.0000	00:55:00	18.0000	00:55:00	43.0000
01:00:00	3.0000	01:00:00	5.0000	01:00:00	6.0000	01:00:00	19.0000	01:00:00	44.0000
01:05:00	3.0000	01:05:00	5.0000	01:05:00	6.0000	01:05:00	20.0000	01:05:00	43.0000
01:10:00	3.0000	01:10:00	5.0000	01:10:00	6.0000	01:10:00	19.0000	01:10:00	45.0000
01:15:00	3.0000	01:15:00	5.0000	01:15:00	6.0000	01:15:00	20.0000	01:15:00	45.0000
01:20:00	3.0000	01:20:00	4.0000	01:20:00	7.0000	01:20:00	17.0000	01:20:00	45.0000
01:25:00	3.0000	01:25:00	4.0000	01:25:00	6.0000	01:25:00	18.0000	01:25:00	44.0000
01:30:00	2.0000	01:30:00	4.0000	01:30:00	6.0000	01:30:00	19.0000	01:30:00	44.0000

23-Time_032-001	24-Turbidity_032-001	25-Time_032-003	26-Turbidity_032-003	27-Time_032-010	28-Turbidity_032-010	29-Time_032-032	30-Turbidity_032-032	31-Time_032-100	32-Turbidity_032-100
00:00:25	0.0000	00:00:25	0.0000	00:00:30	3.0000	00:00:26	3.0000	00:00:29	11.0000
00:05:00	0.0000	00:05:00	3.0000	00:05:00	12.0000	00:05:00	27.0000	00:05:00	33.0000
00:10:00	1.0000	00:10:00	7.0000	00:10:00	22.0000	00:10:00	41.0000	00:10:00	47.0000
00:15:00	0.0000	00:15:00	7.0000	00:15:00	22.0000	00:15:00	46.0000	00:15:00	54.0000
00:20:00	0.0000	00:20:00	6.0000	00:20:00	23.0000	00:20:00	51.0000	00:20:00	61.0000
00:25:00	1.0000	00:25:00	8.0000	00:25:00	26.0000	00:25:00	57.0000	00:25:00	69.0000
00:30:00	0.0000	00:30:00	6.0000	00:30:00	22.0000	00:30:00	59.0000	00:30:00	73.0000
00:35:00	0.0000	00:35:00	6.0000	00:35:00	24.0000	00:35:00	62.0000	00:35:00	78.0000
00:40:00	1.0000	00:40:00	7.0000	00:40:00	25.0000	00:40:00	66.0000	00:40:00	83.0000
00:45:00	0.0000	00:45:00	7.0000	00:45:00	25.0000	00:45:00	68.0000	00:45:00	88.0000
00:50:00	0.0000	00:50:00	7.0000	00:50:00	24.0000	00:50:00	69.0000	00:50:00	90.0000
00:55:00	2.0000	00:55:00	8.0000	00:55:00	25.0000	00:55:00	72.0000	00:55:00	96.0000
01:00:00	0.0000	01:00:00	6.0000	01:00:00	23.0000	01:00:00	71.0000	01:00:00	98.0000
01:05:00	0.0000	01:05:00	7.0000	01:05:00	24.0000	01:05:00	72.0000	01:05:00	101.0000
01:10:00	2.0000	01:10:00	10.0000	01:10:00	25.0000	01:10:00	74.0000	01:10:00	104.0000
01:15:00	0.0000	01:15:00	6.0000	01:15:00	23.0000	01:15:00	74.0000	01:15:00	108.0000
01:20:00	1.0000	01:20:00	7.0000	01:20:00	24.0000	01:20:00	74.0000	01:20:00	111.0000
01:25:00	1.0000	01:25:00	7.0000	01:25:00	25.0000	01:25:00	73.0000	01:25:00	113.0000
01:30:00	0.0000	01:30:00	7.0000	01:30:00	25.0000	01:30:00	73.0000	01:30:00	117.0000
01:35:00	0.0000	01:35:00	6.0000	01:35:00	23.0000	01:35:00	72.0000	01:35:00	116.0000
01:40:00	1.0000	01:40:00	6.0000	01:40:00	23.0000	01:40:00	72.0000	01:40:00	119.0000
01:45:00	1.0000	01:45:00	7.0000	01:45:00	23.0000	01:45:00	73.0000	01:45:00	123.0000
01:50:00	2.0000	01:50:00	8.0000	01:50:00	25.0000	01:50:00	74.0000	01:50:00	125.0000
01:55:00	1.0000	01:55:00	8.0000	01:55:00	24.0000	01:55:00	74.0000	01:55:00	128.0000
02:00:00	0.0000	02:00:00	7.0000	02:00:00	24.0000	02:00:00	72.0000	02:00:00	128.0000
02:05:00	0.0000	02:05:00	6.0000	02:05:00	23.0000	02:05:00	72.0000	02:05:00	130.0000
02:10:00	0.0000	02:10:00	8.0000	02:10:00	23.0000	02:10:00	72.0000	02:10:00	130.0000
02:15:00	0.0000	02:15:00	6.0000	02:15:00	23.0000	02:15:00	71.0000	02:15:00	132.0000
02:20:00	1.0000	02:20:00	8.0000	02:20:00	25.0000	02:20:00	73.0000	02:20:00	135.0000
02:25:00	0.0000	02:25:00	5.0000	02:25:00	22.0000	02:25:00	71.0000	02:25:00	134.0000
02:30:00	0.0000	02:30:00	6.0000	02:30:00	23.0000	02:30:00	71.0000	02:30:00	136.0000
02:35:00	0.0000	02:35:00	7.0000	02:35:00	23.0000	02:35:00	72.0000	02:35:00	136.0000
02:40:00	1.0000	02:40:00	9.0000	02:40:00	25.0000	02:40:00	73.0000	02:40:00	139.0000
02:45:00	0.0000	02:45:00	5.0000	02:45:00	23.0000	02:45:00	71.0000	02:45:00	138.0000
02:50:00	0.0000	02:50:00	7.0000	02:50:00	23.0000	02:50:00	71.0000	02:50:00	138.0000
02:55:00	0.0000	02:55:00	7.0000	02:55:00	23.0000	02:55:00	71.0000	02:55:00	141.0000
03:00:00	2.0000	03:00:00	8.0000	03:00:00	25.0000	03:00:00	72.0000	03:00:00	141.0000
03:05:00	0.0000	03:05:00	7.0000	03:05:00	23.0000	03:05:00	70.0000	03:05:00	139.0000
03:10:00	0.0000	03:10:00	6.0000	03:10:00	23.0000	03:10:00	70.0000	03:10:00	140.0000
03:15:00	0.0000	03:15:00	6.0000	03:15:00	23.0000	03:15:00	70.0000	03:15:00	142.0000
03:20:00	0.0000	03:20:00	6.0000	03:20:00	23.0000	03:20:00	69.0000	03:20:00	140.0000
03:25:00	0.0000	03:25:00	7.0000	03:25:00	23.0000	03:25:00	70.0000	03:25:00	141.0000
03:30:00	0.0000	03:30:00	6.0000	03:30:00	23.0000	03:30:00	69.0000	03:30:00	139.0000
03:35:00	0.0000	03:35:00	7.0000	03:35:00	24.0000	03:35:00	69.0000	03:35:00	142.0000
03:40:00	1.0000	03:40:00	7.0000	03:40:00	24.0000	03:40:00	70.0000	03:40:00	138.0000
03:45:00	0.0000	03:45:00	6.0000	03:45:00	23.0000	03:45:00	69.0000	03:45:00	137.0000
03:50:00	0.0000	03:50:00	6.0000	03:50:00	22.0000	03:50:00	67.0000	03:50:00	121.0000
03:55:00	0.0000	03:55:00	5.0000	03:55:00	23.0000	03:55:00	67.0000	03:55:00	119.0000
04:00:00	0.0000	04:00:00	6.0000	04:00:00	23.0000	04:00:00	67.0000	04:00:00	117.0000
04:05:00	0.0000	04:05:00	7.0000	04:05:00	24.0000	04:05:00	67.0000	04:05:00	112.0000
04:10:00	0.0000	04:10:00	7.0000	04:10:00	23.0000	04:10:00	66.0000	04:10:00	111.0000
04:15:00	0.0000	04:15:00	7.0000	04:15:00	23.0000	04:15:00	64.0000	04:15:00	108.0000
04:20:00	0.0000	04:20:00	6.0000	04:20:00	23.0000	04:20:00	65.0000	04:20:00	99.0000
04:25:00	0.0000	04:25:00	6.0000	04:25:00	22.0000	04:25:00	65.0000	04:25:00	97.0000
04:30:00	0.0000	04:30:00	6.0000	04:30:00	22.0000	04:30:00	63.0000	04:30:00	101.0000
04:35:00	0.0000	04:35:00	6.0000	04:35:00	23.0000	04:35:00	62.0000	04:35:00	93.0000

34-Time_100-001	35-Turbidity_100-001	36-Time_100-003	37-Turbidity_100-003	38-Time_100-010	39-Turbidity_100-010	40-Time_100-032	41-Turbidity_100-032	42-Time_100-100	43-Turbidity_100-100
00:00:25	2.0000	00:00:32	3.0000	00:00:27	8.0000	00:00:24	12.0000	00:00:34	11.0000
00:05:00	3.0000	00:05:00	12.0000	00:05:00	38.0000	00:05:00	52.0000	00:05:00	51.0000
00:10:00	6.0000	00:10:00	20.0000	00:10:00	52.0000	00:10:00	74.0000	00:10:00	71.0000
00:15:00	8.0000	00:15:00	23.0000	00:15:00	60.0000	00:15:00	88.0000	00:15:00	88.0000
00:20:00	8.0000	00:20:00	24.0000	00:20:00	65.0000	00:20:00	100.0000	00:20:00	105.0000
00:25:00	9.0000	00:25:00	24.0000	00:25:00	70.0000	00:25:00	108.0000	00:25:00	116.0000
00:30:00	8.0000	00:30:00	23.0000	00:30:00	73.0000	00:30:00	117.0000	00:30:00	125.0000
00:35:00	8.0000	00:35:00	24.0000	00:35:00	75.0000	00:35:00	125.0000	00:35:00	132.0000
00:40:00	9.0000	00:40:00	24.0000	00:40:00	79.0000	00:40:00	133.0000	00:40:00	143.0000
00:45:00	7.0000	00:45:00	24.0000	00:45:00	81.0000	00:45:00	140.0000	00:45:00	149.0000
00:50:00	8.0000	00:50:00	25.0000	00:50:00	82.0000	00:50:00	146.0000	00:50:00	153.0000
00:55:00	8.0000	00:55:00	24.0000	00:55:00	83.0000	00:55:00	156.0000	00:55:00	156.0000
01:00:00	8.0000	01:00:00	24.0000	01:00:00	84.0000	01:00:00	153.0000	01:00:00	157.0000
01:05:00	8.0000	01:05:00	23.0000	01:05:00	85.0000	01:05:00	160.0000	01:05:00	162.0000
01:10:00	8.0000	01:10:00	24.0000	01:10:00	86.0000	01:10:00	160.0000	01:10:00	170.0000
01:15:00	8.0000	01:15:00	24.0000	01:15:00	87.0000	01:15:00	164.0000	01:15:00	171.0000
01:20:00	8.0000	01:20:00	23.0000	01:20:00	87.0000	01:20:00	167.0000	01:20:00	174.0000
01:25:00	8.0000	01:25:00	24.0000	01:25:00	88.0000	01:25:00	170.0000	01:25:00	177.0000
01:30:00	9.0000	01:30:00	25.0000	01:30:00	89.0000	01:30:00	174.0000	01:30:00	179.0000
01:35:00	8.0000	01:35:00	23.0000	01:35:00	89.0000	01:35:00	178.0000	01:35:00	180.0000
01:40:00	8.0000	01:40:00	24.0000	01:40:00	90.0000	01:40:00	179.0000	01:40:00	182.0000
01:45:00	9.0000	01:45:00	24.0000	01:45:00	90.0000	01:45:00	182.0000	01:45:00	184.0000
01:50:00	8.0000	01:50:00	24.0000	01:50:00	90.0000	01:50:00	183.0000	01:50:00	184.0000
01:55:00	8.0000	01:55:00	24.0000	01:55:00	90.0000	01:55:00	184.0000	01:55:00	186.0000
02:00:00	8.0000	02:00:00	24.0000	02:00:00	91.0000	02:00:00	186.0000	02:00:00	182.0000
02:05:00	9.0000	02:05:00	24.0000	02:05:00	91.0000	02:05:00	188.0000	02:05:00	183.0000
02:10:00	8.0000	02:10:00	24.0000	02:10:00	91.0000	02:10:00	183.0000	02:10:00	180.0000
02:15:00	8.0000	02:15:00	24.0000	02:15:00	91.0000	02:15:00	188.0000	02:15:00	176.0000
02:20:00	7.0000	02:20:00	24.0000	02:20:00	90.0000	02:20:00	186.0000	02:20:00	161.0000
02:25:00	9.0000	02:25:00	24.0000	02:25:00	91.0000	02:25:00	189.0000	02:25:00	161.0000
02:30:00	8.0000	02:30:00	24.0000	02:30:00	91.0000	02:30:00	177.0000	02:30:00	165.0000
02:35:00	8.0000	02:35:00	24.0000	02:35:00	90.0000	02:35:00	178.0000	02:35:00	139.0000
02:40:00	8.0000	02:40:00	23.0000	02:40:00	89.0000	02:40:00	176.0000	02:40:00	127.0000
02:45:00	8.0000	02:45:00	24.0000	02:45:00	90.0000	02:45:00	150.0000	02:45:00	112.0000
02:50:00	9.0000	02:50:00	24.0000	02:50:00	90.0000	02:50:00	152.0000	02:50:00	105.0000
02:55:00	8.0000	02:55:00	24.0000	02:55:00	89.0000	02:55:00	135.0000	02:55:00	100.0000
03:00:00	8.0000	03:00:00	24.0000	03:00:00	88.0000	03:00:00	132.0000	03:00:00	97.0000
03:05:00	8.0000	03:05:00	24.0000	03:05:00	89.0000	03:05:00	121.0000	03:05:00	96.0000
03:10:00	8.0000	03:10:00	24.0000	03:10:00	88.0000	03:10:00	125.0000	03:10:00	90.0000
03:15:00	8.0000	03:15:00	24.0000	03:15:00	88.0000	03:15:00	115.0000	03:15:00	86.0000
03:20:00	7.0000	03:20:00	24.0000	03:20:00	87.0000	03:20:00	99.0000	03:20:00	88.0000
03:25:00	7.0000	03:25:00	23.0000	03:25:00	86.0000	03:25:00	97.0000	03:25:00	86.0000
03:30:00	7.0000	03:30:00	24.0000	03:30:00	85.0000	03:30:00	97.0000	03:30:00	78.0000

45-Time_317-001	46-Turbidity_317-001	47-Time_317-003	48-Turbidity_317-003	49-Time_317-010	50-Turbidity_317-010	51-Time_317-032	52-Turbidity_317-032	53-Time_317-100	54-Turbidity_317-100
00:00:36	0.0000	00:00:28	6.0000	00:00:25	9.0000	00:00:26	21.0000	00:00:30	20.0000
00:05:00	8.0000	00:05:00	33.0000	00:05:00	57.0000	00:05:00	84.0000	00:05:00	84.0000
00:10:00	14.0000	00:10:00	47.0000	00:10:00	85.0000	00:10:00	119.0000	00:10:00	124.0000
00:15:00	19.0000	00:15:00	56.0000	00:15:00	98.0000	00:15:00	143.0000	00:15:00	150.0000
00:20:00	19.0000	00:20:00	62.0000	00:20:00	112.0000	00:20:00	160.0000	00:20:00	160.0000
00:25:00	20.0000	00:25:00	65.0000	00:25:00	122.0000	00:25:00	175.0000	00:25:00	179.0000
00:30:00	20.0000	00:30:00	67.0000	00:30:00	131.0000	00:30:00	186.0000	00:30:00	188.0000
00:35:00	20.0000	00:35:00	71.0000	00:35:00	139.0000	00:35:00	197.0000	00:35:00	197.0000
00:40:00	20.0000	00:40:00	73.0000	00:40:00	146.0000	00:40:00	205.0000	00:40:00	203.0000
00:45:00	20.0000	00:45:00	74.0000	00:45:00	152.0000	00:45:00	213.0000	00:45:00	208.0000
00:50:00	19.0000	00:50:00	75.0000	00:50:00	156.0000	00:50:00	219.0000	00:50:00	212.0000
00:55:00	20.0000	00:55:00	77.0000	00:55:00	162.0000	00:55:00	227.0000	00:55:00	217.0000
01:00:00	21.0000	01:00:00	79.0000	01:00:00	168.0000	01:00:00	232.0000	01:00:00	220.0000
01:05:00	19.0000	01:05:00	79.0000	01:05:00	173.0000	01:05:00	237.0000	01:05:00	223.0000
01:10:00	20.0000	01:10:00	80.0000	01:10:00	179.0000	01:10:00	243.0000	01:10:00	225.0000
01:15:00	21.0000	01:15:00	82.0000	01:15:00	187.0000	01:15:00	247.0000	01:15:00	228.0000
01:20:00	20.0000	01:20:00	83.0000	01:20:00	195.0000	01:20:00	251.0000	01:20:00	231.0000
01:25:00	20.0000	01:25:00	82.0000	01:25:00	194.0000	01:25:00	254.0000	01:25:00	231.0000
01:30:00	20.0000	01:30:00	83.0000	01:30:00	200.0000	01:30:00	257.0000	01:30:00	231.0000
01:35:00	21.0000	01:35:00	84.0000	01:35:00	203.0000	01:35:00	260.0000	01:35:00	235.0000
01:40:00	21.0000	01:40:00	84.0000	01:40:00	207.0000	01:40:00	263.0000	01:40:00	233.0000
01:45:00	19.0000	01:45:00	85.0000	01:45:00	212.0000	01:45:00	265.0000	01:45:00	235.0000
01:50:00	19.0000	01:50:00	82.0000	01:50:00	215.0000	01:50:00	264.0000	01:50:00	235.0000
01:55:00	21.0000	01:55:00	85.0000	01:55:00	217.0000	01:55:00	263.0000	01:55:00	236.0000
02:00:00	21.0000	02:00:00	85.0000	02:00:00	218.0000	02:00:00	263.0000	02:00:00	229.0000
02:05:00	20.0000	02:05:00	84.0000	02:05:00	218.0000	02:05:00	271.0000	02:05:00	231.0000
02:10:00	21.0000	02:10:00	85.0000	02:10:00	222.0000	02:10:00	271.0000	02:10:00	233.0000
02:15:00	20.0000	02:15:00	86.0000	02:15:00	219.0000	02:15:00	271.0000	02:15:00	229.0000
02:20:00	21.0000	02:20:00	86.0000	02:20:00	217.0000	02:20:00	272.0000	02:20:00	227.0000
02:25:00	20.0000	02:25:00	86.0000	02:25:00	225.0000	02:25:00	272.0000	02:25:00	225.0000
02:30:00	20.0000	02:30:00	84.0000	02:30:00	227.0000	02:30:00	263.0000	02:30:00	221.0000
02:35:00	20.0000	02:35:00	84.0000	02:35:00	227.0000	02:35:00	258.0000	02:35:00	201.0000
02:40:00	20.0000	02:40:00	86.0000	02:40:00	224.0000	02:40:00	228.0000	02:40:00	199.0000
02:45:00	19.0000	02:45:00	84.0000	02:45:00	227.0000	02:45:00	223.0000	02:45:00	187.0000
02:50:00	19.0000	02:50:00	84.0000	02:50:00	218.0000	02:50:00	212.0000	02:50:00	185.0000
02:55:00	20.0000	02:55:00	85.0000	02:55:00	217.0000	02:55:00	208.0000	02:55:00	177.0000
03:00:00	20.0000	03:00:00	84.0000	03:00:00	219.0000	03:00:00	186.0000	03:00:00	167.0000

56-Time_700-001	57-Turbidity_700-001	58-Time_700-003	59-Turbidity_700-003	60-Time_700-010	61-Turbidity_700-010	62-Time_700-032	63-Turbidity_700-032	64-Time_700-100	65-Turbidity_700-100
00:00:25	7.0000	00:00:28	12.0000	00:00:27	19.0000	00:00:22	26.0000	00:00:27	35.0000
00:05:00	34.0000	00:05:00	61.0000	00:05:00	92.0000	00:05:00	113.0000	00:05:00	123.0000
00:10:00	45.0000	00:10:00	85.0000	00:10:00	131.0000	00:10:00	157.0000	00:10:00	167.0000
00:15:00	54.0000	00:15:00	100.0000	00:15:00	156.0000	00:15:00	186.0000	00:15:00	191.0000
00:20:00	58.0000	00:20:00	111.0000	00:20:00	176.0000	00:20:00	207.0000	00:20:00	205.0000
00:25:00	61.0000	00:25:00	121.0000	00:25:00	192.0000	00:25:00	223.0000	00:25:00	214.0000
00:30:00	61.0000	00:30:00	128.0000	00:30:00	206.0000	00:30:00	235.0000	00:30:00	220.0000
00:35:00	65.0000	00:35:00	135.0000	00:35:00	218.0000	00:35:00	245.0000	00:35:00	225.0000
00:40:00	66.0000	00:40:00	140.0000	00:40:00	231.0000	00:40:00	254.0000	00:40:00	227.0000
00:45:00	67.0000	00:45:00	147.0000	00:45:00	238.0000	00:45:00	262.0000	00:45:00	229.0000
00:50:00	66.0000	00:50:00	152.0000	00:50:00	248.0000	00:50:00	267.0000	00:50:00	230.0000
00:55:00	68.0000	00:55:00	157.0000	00:55:00	255.0000	00:55:00	275.0000	00:55:00	231.0000
01:00:00	69.0000	01:00:00	159.0000	01:00:00	268.0000	01:00:00	277.0000	01:00:00	232.0000
01:05:00	70.0000	01:05:00	163.0000	01:05:00	278.0000	01:05:00	279.0000	01:05:00	231.0000
01:10:00	68.0000	01:10:00	167.0000	01:10:00	276.0000	01:10:00	280.0000	01:10:00	228.0000
01:15:00	68.0000	01:15:00	169.0000	01:15:00	282.0000	01:15:00	281.0000	01:15:00	230.0000
01:20:00	69.0000	01:20:00	173.0000	01:20:00	286.0000	01:20:00	278.0000	01:20:00	232.0000
01:25:00	68.0000	01:25:00	173.0000	01:25:00	286.0000	01:25:00	274.0000	01:25:00	229.0000
01:30:00	70.0000	01:30:00	177.0000	01:30:00	289.0000	01:30:00	267.0000	01:30:00	230.0000
01:35:00	70.0000	01:35:00	179.0000	01:35:00	293.0000	01:35:00	260.0000	01:35:00	229.0000
01:40:00	69.0000	01:40:00	181.0000	01:40:00	297.0000	01:40:00	232.0000	01:40:00	231.0000
01:45:00	68.0000	01:45:00	183.0000	01:45:00	298.0000	01:45:00	185.0000	01:45:00	227.0000
01:50:00	70.0000	01:50:00	184.0000	01:50:00	289.0000	01:50:00	167.0000	01:50:00	224.0000
01:55:00	69.0000	01:55:00	185.0000	01:55:00	298.0000	01:55:00	151.0000	01:55:00	224.0000
02:00:00	70.0000	02:00:00	186.0000	02:00:00	300.0000	02:00:00	136.0000	02:00:00	215.0000
02:05:00	70.0000	02:05:00	188.0000	02:05:00	293.0000	02:05:00	127.0000	02:05:00	220.0000
02:10:00	70.0000	02:10:00	188.0000	02:10:00	275.0000	02:10:00	117.0000	02:10:00	208.0000
02:15:00	70.0000	02:15:00	189.0000	02:15:00	254.0000	02:15:00	110.0000	02:15:00	202.0000
02:20:00	70.0000	02:20:00	191.0000	02:20:00	227.0000	02:20:00	115.0000	02:20:00	197.0000
02:25:00	69.0000	02:25:00	191.0000	02:25:00	211.0000	02:25:00	111.0000	02:25:00	181.0000

3. Turbidity (FAU and NTU), EC ($mScm^{-1}$) and Total Fe (mgL^{-1}) measurements for tank experiments:

1-Time 42.2-010	2-Turbidity(NTU) 42.2-010	3-Turbidity(FAU) 42.2-010	4-EC 42.21-010	5-Fe(tot) 42.2-010	6
00:00:00	5.4500	5.0000	44.3000	0.0700	
00:05:00	18.5000	30.0000	41.0333	3.2400	
00:30:00	16.6000	28.0000	40.7667	3.7800	
01:00:00	15.9000	28.0000	41.0000	3.8400	
01:30:00	16.0000	29.0000	40.9000	3.7200	
02:00:00	15.6000	29.0000	41.2000	3.8400	
02:30:00	15.5000	30.0000	40.7000	3.7400	
03:00:00	15.5000	28.0000	40.8000	3.8400	
03:30:00	15.3000	29.0000	40.5667	3.8000	
04:00:00	15.2000	29.0000	40.7000	3.8000	
04:30:00	15.1000	29.0000	40.4000	3.8000	
05:00:00	15.1000	29.0000	40.5333	3.7800	
05:30:00	15.0000	29.0000	40.7000	3.7800	
06:00:00	15.1000	29.0000	40.6667	3.8600	
20:00:00	3.2300	6.0000	38.9333	0.8200	

7-Time 100-010	8-Turbidity(NTU) 100-010	9-Turbidity(FAU) 100-010	10-EC 100-010	11-Fe(tot) 100-010	12
00:00:00	1.5900	1.0000	45.1333	0.0800	
00:05:00	38.1000	62.0000	43.0667	8.8400	
00:30:00	37.4000	60.0000	42.5333	8.8000	
01:00:00	37.5000	62.0000	42.4667	8.7600	
01:30:00	37.6000	61.0000	42.7000	8.7600	
02:00:00	37.2000	60.0000	43.4667	8.7200	
02:30:00	37.0000	60.0000	43.1000	8.6800	
03:00:00	36.8000	60.0000	42.4333	8.6400	
03:30:00	36.6000	61.0000	44.8000	8.6400	
04:00:00	36.8000	61.0000	43.6667	8.6400	
04:30:00	36.2000	59.0000	42.2667	8.4800	
05:00:00	35.2000	57.0000	43.1667	8.2400	
05:30:00	33.9000	54.0000	43.2000	8.0800	
06:00:00	31.1000	53.0000	43.3667	5.9600	
22:00:00	3.7800	6.0000	43.1000	0.8400	

13-Time 136.2-010	14-Turbidity(NTU) 136.2-010	15-Turbidity(FAU) 136.2-010	16-EC 136.2-010	17-Fe(tot) 136.2-010	18
00:05:00	No	71.0000	40.2667	10.8800	
00:30:00	data	74.0000	41.0667	11.1600	
01:00:00	available	79.0000	41.7000	11.2400	
01:30:00	due	78.0000	42.3333	11.2800	
02:00:00	to	80.0000	43.0333	11.3200	
02:30:00	technical	80.0000	43.1333	11.3600	
03:00:00	fault	78.0000	43.4667	11.2400	
03:30:00	in	80.0000	43.6667	11.4400	
04:00:00	instrument.	77.0000	43.6000	11.1200	
04:30:00		66.0000	43.9333	9.3200	
05:00:00		51.0000	43.6667	7.4800	
05:30:00		44.0000	43.8667	6.2400	
06:00:00		39.0000	43.1000	5.4400	
20:00:00		7.0000	42.7333	1.1600	

19-Time 418.14-010	20-Turbidity(NTU) 418.14-010	21-Turbidity(FAU) 418.14-010	22-EC 418.14-010	23-Fe(tot) 418.14-010	24
00:00:00	5.9100	7.0000	42.6000	0.0600	
00:05:00	74.0000	135.0000	39.1333	38.2200	
00:30:00	95.6000	170.0000	40.0000	39.6900	
01:00:00	115.0000	205.0000	40.7333	38.0100	
01:30:00	128.0000	227.0000	40.1333	38.0100	
02:00:00	135.0000	237.0000	40.1000	36.7500	
02:30:00	136.0000	244.0000	39.5000	36.1200	
03:00:00	131.0000	229.0000	39.8667	33.8100	
03:30:00	110.0000	190.0000	40.0667	29.4000	
04:00:00	95.5000	164.0000	39.9667	26.2500	
04:30:00	74.6000	130.0000	39.7000	22.2600	
05:00:00	64.6000	113.0000	39.9000	20.1600	
05:30:00	56.0000	100.0000	39.4333	18.6900	
06:00:00	51.9000	93.0000	40.3667	15.7500	
20:00:00	17.5000	36.0000	39.1667	9.2400	

25-Time 678.0-010	26-Turbidity(NTU) 678.0-010	27-Turbidity(FAU) 678.0-010	28-EC 678.0-010	29-Fe(tot) 678.0-010	30
00:05:00	58.4000	104.0000	38.1667	67.5000	
00:30:00	109.0000	186.0000	38.0333	67.2000	
01:00:00	134.0000	229.0000	38.3333	66.6000	
01:30:00	134.0000	260.0000	37.9333	66.6000	
02:00:00	162.0000	278.0000	37.8333	65.7000	
02:30:00	171.0000	297.0000	37.9667	66.3000	
03:00:00	179.0000	311.0000	38.0667	66.6000	
03:30:00	134.0000	232.0000	38.0000	58.5000	
04:00:00	98.6000	172.0000	38.0000	51.0000	
04:30:00	79.1000	140.0000	38.0667	47.7000	
05:00:00	64.4000	118.0000	37.8667	44.4000	
05:30:00	57.1000	104.0000	38.0667	42.9000	
06:00:00	53.6000	98.0000	38.0000	42.6000	
22:20:00	18.4000	31.0000	37.3333	34.2000	

31-Time_100-050	32-Turbidity(NTU)_100-050	33-Turbidity(FAU)_100-050	34-EC_100-050	35-Fe(tot)_100-050	36
00:05:00	48.3000	67.0000	19.7067	46.6000	
00:30:00	86.7000	122.0000	19.8667	46.0000	
01:00:00	108.0000	152.0000	19.8600	45.8000	
01:30:00	127.0000	177.0000	19.8367	45.8000	
02:00:00	136.0000	189.0000	20.0667	45.6000	
02:30:00	143.0000	201.0000	19.9800	45.4000	
03:00:00	154.0000	212.0000	19.7333	45.4000	
03:30:00	162.0000	219.0000	19.8367	45.2000	
04:00:00	167.0000	227.0000	19.9967	45.4000	
04:30:00	172.0000	235.0000	20.0033	45.2000	
05:00:00	174.0000	237.0000	19.9567	45.0000	
05:30:00	176.0000	233.0000	18.0700	44.6000	
06:00:00	178.0000	239.0000	19.9833	44.2000	
06:30:00	166.0000	223.0000	20.0367	43.0000	
00:00:00	26.4000	36.0000	19.7600	26.0000	

37-Time_678.0-050	38-Turbidity(NTU)_678.0-050	39-Turbidity(FAU)_678.0-050	40-EC_678.0-050	41-Fe(tot)_678.0-050	42
00:05:00	126.0000	195.0000	20.8667	341.7000	
00:30:00	170.0000	256.0000	21.0000	341.7000	
01:00:00	185.0000	277.0000	21.1000	339.6900	
01:30:00	192.0000	291.0000	20.8667	341.7000	
02:00:00	198.0000	297.0000	21.1333	343.7100	
02:30:00	201.0000	303.0000	21.0333	343.7100	
03:00:00	201.0000	301.0000	21.0333	343.7100	
03:30:00	203.0000	304.0000	21.2000	341.7000	
04:00:00	197.0000	294.0000	21.1333	341.7000	
04:30:00	194.0000	289.0000	21.0000	341.7000	
05:00:00	167.0000	249.0000	21.0000	337.6800	
05:30:00	144.0000	213.0000	21.1667	335.6700	
06:00:00	129.0000	192.0000	21.1667	333.6600	
20:00:00	23.5000	36.0000	20.7667	323.6100	